

**SECOND EUROPEAN SUMMER SCHOOL on  
MICROSCOPIC QUANTUM MANY-BODY THEORIES  
and their APPLICATIONS**

**(3 - 14 September 2001)**

---

**THEORETICAL ASPECTS OF THE  
BOSE-EINSTEIN CONDENSATION**

**Adelchi FABROCINI  
Dipartimento di Fisica  
Universita' di Pisa  
Via Buonarroti, 2 - Ed. B  
I-56127 Pisa  
ITALY**

---

These are preliminary lecture notes, intended only for distribution to participants



A basic (sometimes trivial)

description of

Bose-Einstein Condensation (BEC)

① Free gas is trapped

Temperature

$$J_{ij} = 0$$

② Homog. Bose gas ("He and H<sub>2</sub>)

Atoms in a trap and clusters

$$J_{ij} \neq 0$$

BEC → macroscopic ( $N_0 \sim N$ ) occupation  
of the lowest lying S.P. energy  
state as  $T \rightarrow 0^{\circ}\text{K}$  (below  $T_c$ ) for Bosons

Homog. systems in  $N \rightarrow \infty$   $\Omega \rightarrow \infty$   $\frac{N}{\Omega} = \rho = \text{const}$   
Hom. therm. li.

$^4\text{He}$  (liquid) pions in nuclear matter  
Cooper pairs excitons etc.

Difficult to spot expt. signatures (direct)

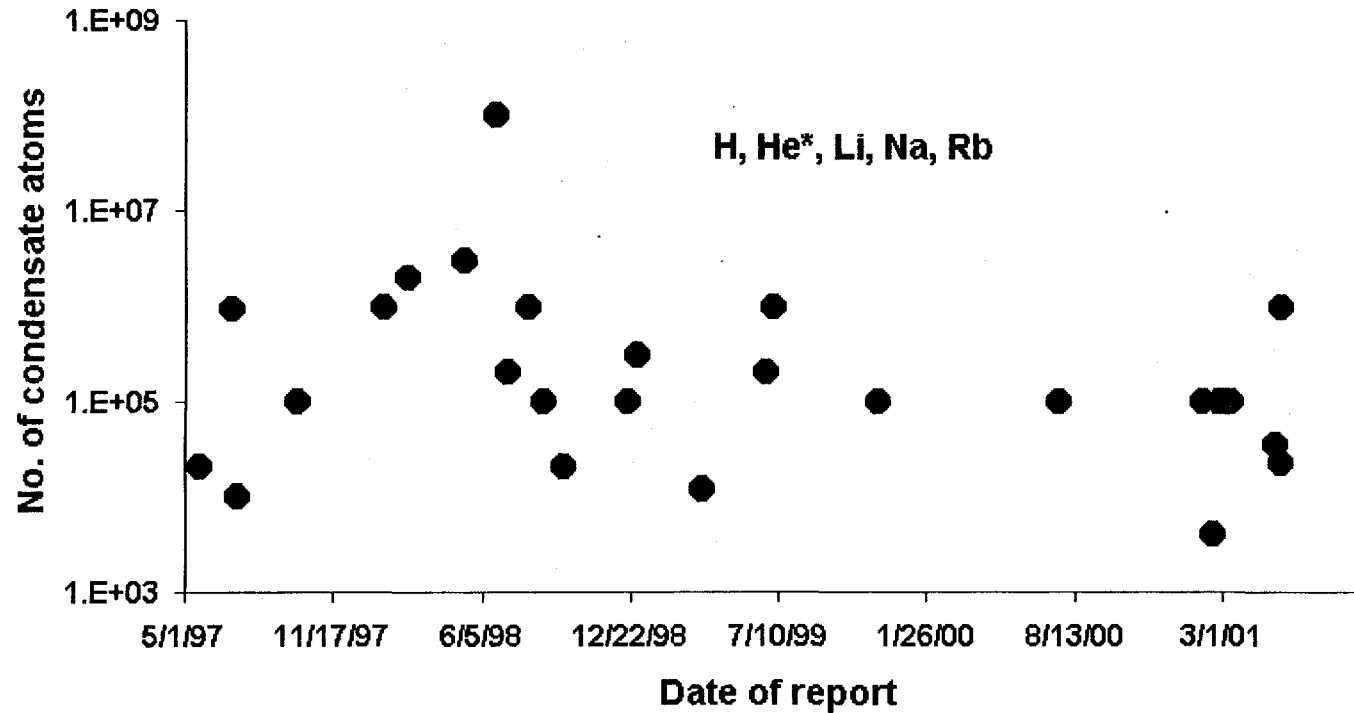
Finite systems inhomog. therm. limit?

Clusters of  $^4\text{He}$  atoms

Alkali atoms in harmonic trap

↑ strikingly clear evidence of BEC

|| BEC from symmetry of the w.f. ||  
(not the interaction)



The BEC actors

New BEC observations from May 1, 1997, as reported by our correspondents. Color indicates atomic species: H, He\*, Li, Na, Rb. Numbers of condensate atoms are as communicated to us, and reflect different thermodynamic conditions - see the original reports for details.

Twenty-six new reports of laboratory observations of BEC in atomic gases have come in since May, 1997:

- May 18, 2001: Vive la difference!
- May 17, 2001: Strine debut

$$\boxed{U_{ij} = 0 \quad T = 0^{\circ}K}$$

homog. Bose gas in the therm. li.

S.P. states  $\Rightarrow$  pl. waves

$$f_{\vec{k}}(\vec{r}_i) = \frac{1}{\sqrt{\Omega}} e^{i\vec{k} \cdot \vec{r}_i}$$

$$\boxed{\Psi(\vec{r}_1, \dots, \vec{r}_N) = \prod_i f(\vec{r}_i)}$$

at condensation  $N_0 = N$  in  $f_0(\vec{r}_i) = \text{const.} = \frac{1}{\sqrt{\Omega}}$   
 $k=0$  state

$$\underline{\Psi_0(N) = C.}$$

In coordinate space  $\rightarrow$  homog. filled by  $|\Psi_0|^2$

One Body Density Matrix (OBDM)

$$\rho_1(\vec{r}_1, \vec{r}_1') = N \int d^3r_2 \dots \int d^3r_N \Psi_0^*(\vec{r}_1, \dots, \vec{r}_N) \Psi_0(\vec{r}_1, \dots, \vec{r}_N) =$$

$$= \text{const} \leftarrow \text{LRD everywhere}$$

One Body Density (OBD)

$$\rho(\vec{r}_1) = \rho_1(\vec{r}_1, \vec{r}_1' = \vec{r}_1) = \frac{N}{\Omega} = \text{const.}$$

Momentum Distribution (MD)

$$n_{\vec{k}} = \int d^3r_1 \int d^3r_1' e^{i\vec{k} \cdot (\vec{r}_1 - \vec{r}_1')} \rho_1(\vec{r}_1, \vec{r}_1') = \delta_{\vec{k}}$$

Flat distribution in coordinate space

$\delta_{\vec{k}=0}$  distribution in mom. space (BEC in  $\vec{k}$ )

# Non homog. (finite systems) Bose gas

Bosons in an external confining potential  
(Harmonic)

Spherical traps (optical or magnetic)

$$\bar{V}_{\text{ext}}(\vec{r}_i) = \frac{1}{2} m_i (\omega_{HO}^2) r_i^2$$

$\omega_{HO}$  = trapping frequency

$$a_{HO}^2 = \frac{\hbar}{m_i \omega_{HO}} = \frac{\hbar^2}{m_i} \frac{1}{\hbar \omega_{HO}}$$

HO length ( $a_{HO}$ )

Many Body Hamiltonian (non interacting)

$$H = -\sum_i \frac{\hbar^2 \nabla_i^2}{2m} + \sum_i \frac{1}{2} m \omega_{HO}^2 r_i^2 = \sum_i h_i$$

Solve  $H_i$  one-body  $h_i$

$$\left( -\frac{\hbar^2}{2m} \nabla^2 + \frac{1}{2} m \omega_{HO}^2 r^2 \right) \varphi_n(\vec{r}) = \epsilon_n \varphi_n(\vec{r})$$

$$\epsilon_n = \left( n_x + n_y + n_z + \frac{3}{2} \right) \hbar \omega_{HO} \quad n_{x,y,z} \geq 0$$

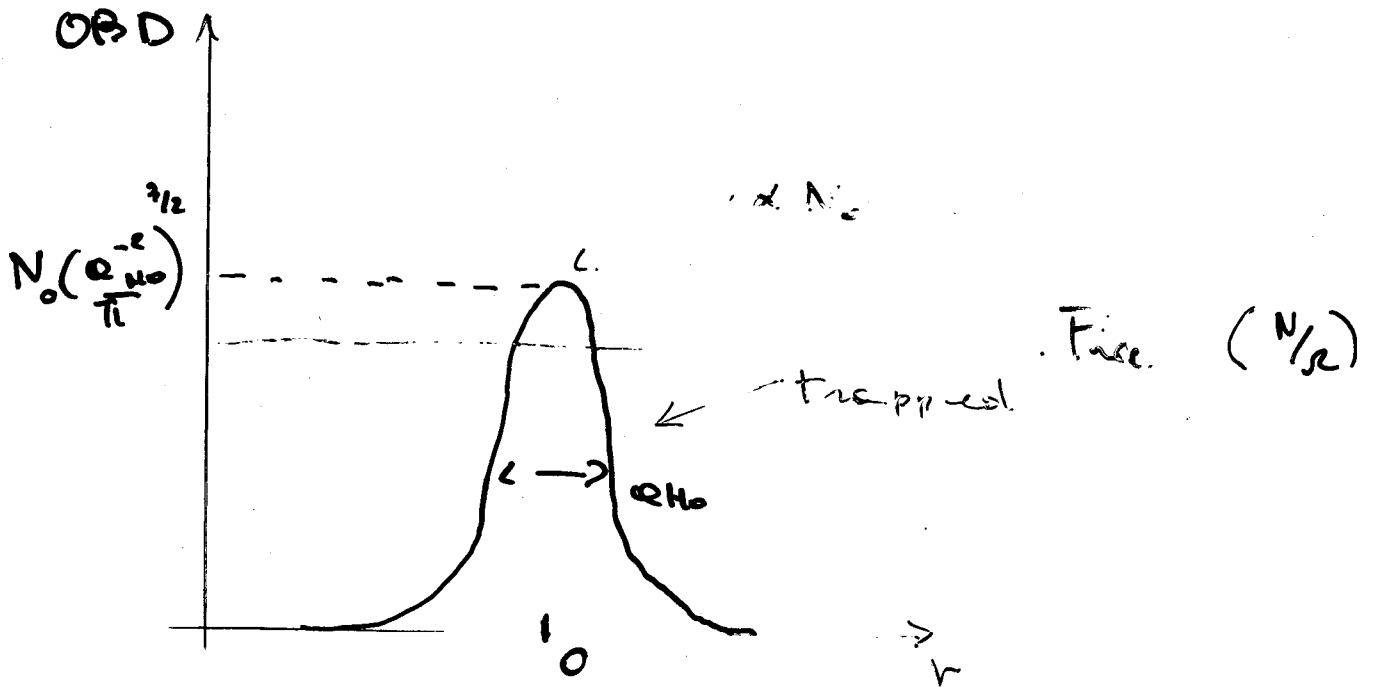
BEC  $\Rightarrow$  All bosons in  $\varphi_0(\vec{r})$  with  $\epsilon_0 = \frac{3}{2} \hbar \omega_{HO}$

$$\boxed{\varphi_0(\vec{r})} = \varphi_0(\vec{r}) = \left( \frac{m_i \omega_{HO}}{\pi \hbar} \right)^{3/4} \exp \left[ -\frac{m_i \omega_{HO}}{2 \hbar} r^2 \right] =$$

$$= \left( \frac{0.4 \text{ nm}^{-1}}{\pi} \right)^{3/4} \exp \left[ -\frac{r^2}{2 a_{HO}^2} \right] \leftarrow$$

$$\int d^3r \varphi_0^2(\vec{r}) = 1$$

$a_{HO} \Rightarrow$  average width of  $|\varphi_0|^2$



OBD  $\Rightarrow \rho(r) = N_0 \left( \frac{L_{HO}^{-2}}{\pi} \right)^{3/2} \exp \left[ -r^2 / L_{HO}^2 \right]$

|| In confined geometries BEC is visible in coordinate space as a peak in the OBD ||

(like exam see it)

CRPH  $\rho_0(\vec{r}_1, \vec{r}_2) = N \left( \frac{L_{HO}^{-2}}{\pi} \right)^{3/2} \exp \left[ -\frac{1}{2} L_{HO}^2 (r_1^2 + r_2^2) \right]$

M.D  $N_{12} = N \left( \frac{L_{HO}^{-2}}{\pi} \right)^{3/2} \exp \left[ -k L_{HO}^2 \right]$



# Shape of trap $\rightarrow$ symmetry of the condensate

Cylindrical external traps

$$V_{\text{ext}}(\vec{r}) = \frac{1}{2} m (\underbrace{\omega_{\perp}^2 r_{\perp}^2}_{\text{radial}} + \underbrace{\omega_z^2 z^2}_{\text{axial}}) \quad r_{\perp}^2 = x^2 + y^2$$

$$\lambda = \frac{\omega_z}{\omega_{\perp}}$$

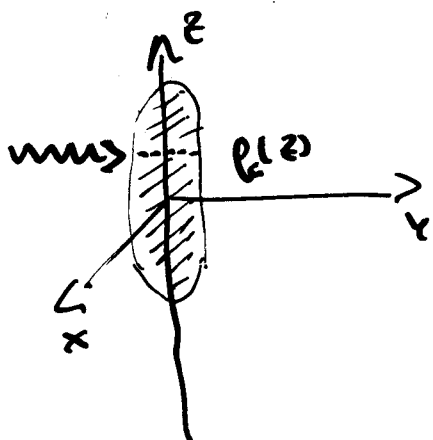
$$E_{n_x, n_y, n_z} = (n_x + n_y + 1) \hbar \omega_{\perp} + (n_z + \frac{1}{2}) \hbar \omega_z$$

$$\psi_0(\vec{r}) = \frac{\lambda^{1/4}}{\pi^{3/4} \omega_{\perp}^{3/2}} \exp \left[ -\frac{\lambda}{2 \omega_{\perp}} (r_{\perp}^2 + \lambda z^2) \right]$$

$$a_{\perp}^2 = \frac{\hbar}{m \omega_{\perp}} \quad \rightarrow \text{H.C. length in } (x, y)$$

1D  $\longleftarrow \lambda > 1$  cigar  
 2D  $\longleftarrow \lambda < 1$  disk

$\Downarrow$  Increase the condensate with a light beam  $\Rightarrow$  Columnar density (optical density)



$$\rho_c(z) = \int dx \rho(x, 0, z)$$

# Turning on the Temperature

$$\beta = 1/k_B T$$

# large T

$$\underline{Z}_0 = \prod_i [1 - e^{-\beta(\mu - \epsilon_i)}]^{-1}$$

$\mu = \text{chem. pot.}$   
 $\epsilon_i = \text{s.p. levels}$

↓

$$\underline{Z}_0 = -k_B T \epsilon_{\mu} \underline{Z}_0 = k_B T \sum_i [1 - e^{-\beta(\mu - \epsilon_i)}]$$

therm. pot.

↓ S, P, N

$$\underline{\langle N \rangle} = - \left( \frac{\partial \Omega_0}{\partial \mu} \right)_{T, \Omega} = \sum_i n_i = \sum_i [e^{-\beta(\mu - \epsilon_i)} - 1]^{-1}$$

## How free Bose gas

$$\begin{aligned} \epsilon_i &\rightarrow \epsilon_k = \frac{\hbar^2 k^2}{2m} \\ \sum_i &\rightarrow \sum_k \rightarrow \frac{\Omega}{(2\pi)^3} \int d^3k \end{aligned}$$

$$DS \rightarrow \rho(\epsilon) = \frac{\Omega}{(2\pi)^3} \left( \frac{2m}{\hbar^2} \right)^{3/2} \epsilon^{1/2}$$

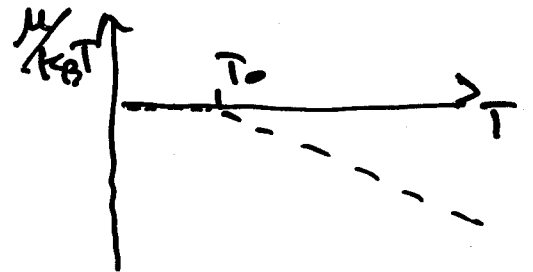
$$E = \sum_i n_i \epsilon_i = \int_0^{\infty} \epsilon \rho(\epsilon) d\epsilon = \int_0^{\infty} \epsilon \rho(\epsilon) d\epsilon / e^{\beta(\epsilon - \mu)} - 1$$

$$\frac{N}{\Omega} = \frac{1}{\Omega} \int_0^{\infty} \rho(\epsilon) d\epsilon / e^{\beta(\epsilon - \mu)} - 1$$

with  $\epsilon - \mu \geq 0$  ( $n_i \geq 0$ )

at  $\epsilon = \epsilon_0 = 0 \Rightarrow \mu \leq 0$

at  $T = T_0$   $\mu(T_0) = 0$



To find  $N = \int_0^{\infty} \rho(\epsilon) d\epsilon / e^{\epsilon/k_B T_0} - 1$

$$T_0 = \frac{\hbar^2}{2m} \frac{1}{k_B} \left[ \frac{4\pi^2}{\Gamma(3/2) \zeta(3/2)} \right]^{2/3} \left( \frac{N}{\Omega} \right)^{2/3} = 3.31 \frac{\hbar^2}{m k_B} \left( \frac{N}{\Omega} \right)^{2/3}$$

In the therm. limit  $\left( \begin{matrix} N \rightarrow \infty \\ \lambda \rightarrow \infty \\ \frac{N}{\lambda} = \text{const} \end{matrix} \right)$

$$\boxed{\bar{T}_c \neq T_c(N)}$$

Above  $T_0$

$N_0 \ll 1$

Below  $T_0$

$N_0 \gg N$

↑  
macrosc. occup. of  $\psi_0$

single occ.  $\psi_0$  at  $T < T_0$

$$N_{\epsilon > \epsilon_0} (\mu = \epsilon) = \frac{N}{\lambda} \left( \frac{T}{T_0} \right)^{3/2}$$

$$\frac{N_0}{\lambda} = \frac{N}{\lambda} - \frac{N_{\epsilon > \epsilon_0}}{\lambda} = \frac{N}{\lambda} \left[ 1 - \left( \frac{T}{T_0} \right)^{3/2} \right] = \frac{N}{\lambda} x_0(T)$$

In  $^4\text{He}$

$$\rho = \frac{N}{\lambda} \approx 145 \text{ g cm}^{-3}$$

$$T_0 = 3.14 \text{ K}$$

$$T_\lambda = 2.2 \text{ K}$$

#

### Confined geometry (HO trap)

$$\epsilon_i \rightarrow \epsilon_n = (n_x + n_y + n_z) \hbar \omega_{HO} + \frac{3}{2} \hbar \omega_{HO}$$

$\underbrace{\hspace{10em}}_{\epsilon_0}$

$$\sum_i \rightarrow \sum_{n_x, n_y, n_z}$$

$$DS \rightarrow \rho(\epsilon) = \frac{1}{2} \frac{1}{(\hbar \omega_{HO})^3} \epsilon^2$$

$$\epsilon - \mu \geq 0 \rightarrow \text{at } \epsilon = \epsilon_0$$

$$\mu = \mu_c = \frac{3}{2} \hbar \omega_{HO}$$

$$N = \sum_{n \neq 0} T_n \beta \hbar \omega_{HO} n \quad T < T_0$$

↓  $N_0 = 1$  at  $T = T_0$

$$N = \int_0^\infty \rho(\epsilon) d\epsilon \Big/ e^{-\frac{\epsilon - \epsilon_0}{k_B T_0}} \Rightarrow \frac{k_B T_0}{\hbar \omega_{HO}} = N^{1/3} / \zeta(3/2)$$

$$k_B T_0 = .94 [N (\hbar \omega_{HO})^3]^{1/3}$$

Thermal limit?

$$\boxed{N \rightarrow \infty \quad \omega_{HO} \rightarrow \infty \quad \text{with } N(\hbar \omega_{HO})^3 = \text{const}}$$

$$T_0 \neq T_0(N)$$

$$\underline{X_0^{\text{class.}}}$$

$$X_0 = 1 - (T/T_0)^3$$

$$\underline{X_0^{\text{quant.}}}$$

$$X_0 = 1 - (T/T_0)^{3/2}$$

Density of particles

thermal particles density

$$\rho(\vec{r}) = \rho_T(\vec{r}) + N_0 |\psi_0(\vec{r})|^2 \quad \text{C.D. of the BEC}$$

$$\rho_T(\vec{r}) = \int d^3p \frac{1}{(2\pi\hbar)^3} \frac{1}{e^{\beta(E_p - \mu)}} \\ = \lambda_T^{-3} g_{3/2}(e^{-\beta(\mu - \epsilon_0)})$$

$$E_p = p^2/2m + \epsilon_0$$

$$\lambda_T = (2\pi\hbar^2 / m k_B T)^{1/2}$$

$$g_{3/2}(z) = \sum_{n=1}^{\infty} z^n \frac{1}{n^{3/2}}$$

Thermal scale of energy

$$k_B T_0 \text{ vs. } \hbar \omega_{HO}$$

$k_B T_0 \sim N^{1/3} \hbar \omega_{HO} \Rightarrow$  at large  $N$  ( $k_B T_0 \gg \hbar \omega_{HO}$ )

semiclassical approx. may work

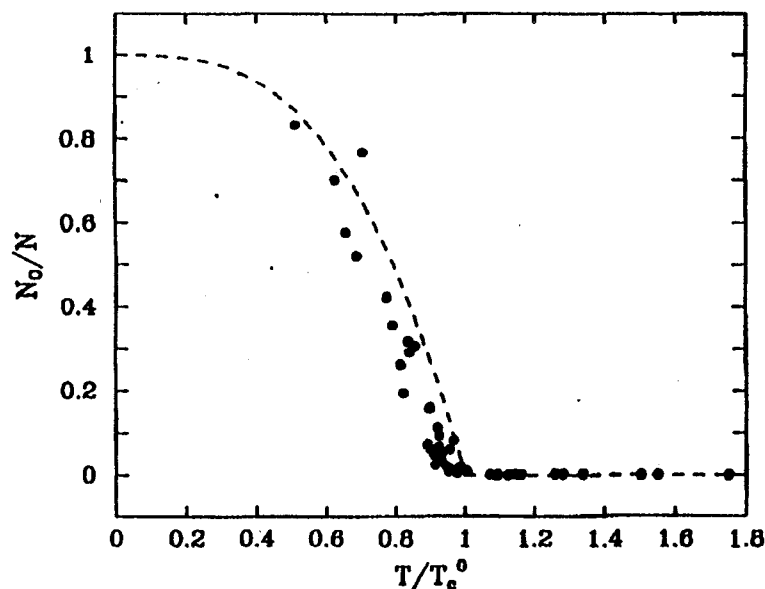


FIG. 5. Condensate fraction as a function of  $T/T_c^0$ . Circles are the experimental results of Ensher *et al.* (1996), while the dashed line is Eq. (15).

analyzed extensively in the next sections. Here we briefly discuss the relevance of finite-size corrections.

### C. Finite-size effects

The number of atoms that can be put into the traps is not truly macroscopic. So far experiments have been carried out with a maximum of about  $10^7$  atoms. As a

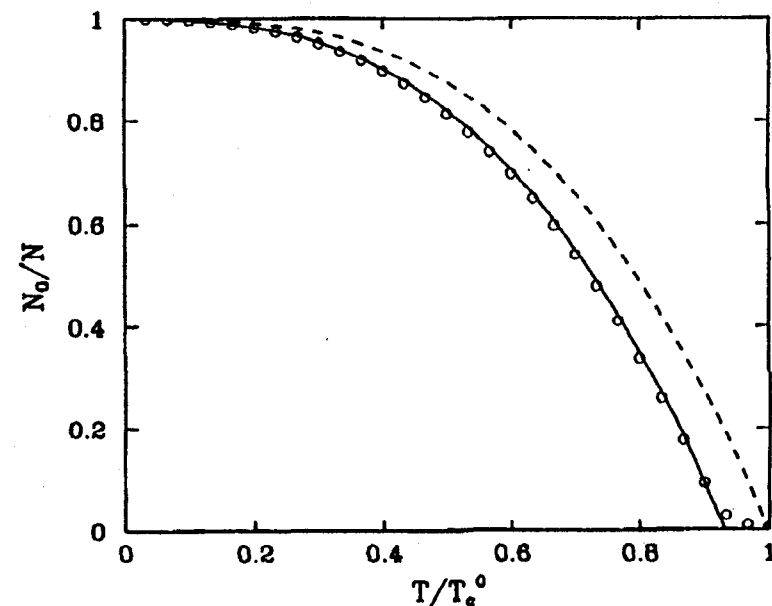


FIG. 6. Condensate fraction vs temperature for an ideal gas in a trap. The circles correspond to the exact quantum calculation for  $N=1000$  atoms in a trap with spherical symmetry and the solid line to the prediction (19). The dashed line refers to the thermodynamic limit (15).

van Druten (1996b) found that finite-size effects are significant only for rather small values of  $N$ , less than about  $10^4$ . They also calculated the occupation of the first excited levels, finding that the fraction of atoms in these states vanishes for  $N \rightarrow \infty$  and is very small already for  $N$  of the order of 100.

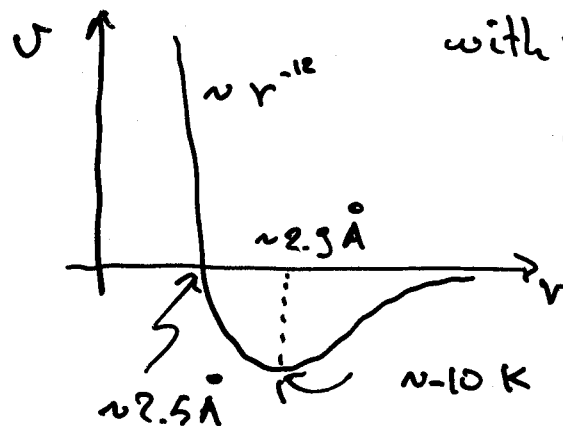
Statistics explains QUALITATIVELY BEC

How about QUANTITATIVELY?

Interaction on!

$$H = -\sum_i \frac{\hbar^2 \nabla_i^2}{2m} + \sum_{i < j} V(r_{ij}) \left( + \sum_i U_{\text{ext}}(\vec{r}_i) \right)$$

a) Large corrections in dense systems ( $^4\text{He}$ )<sup>\*</sup>  
with strong interaction (LJ)



$$r_0 \approx 2.2 \text{ \AA}$$

$$\frac{4}{3} \pi \rho r_0^3 = 1$$

b) Sizeable corrections in dilute systems  
(Hard Spheres, Alkali)

<sup>\*</sup> Ideal playground for battlefield for Many-Body theories (Simple  $\psi$  laws &)

# BEC in liquid $^4\text{He}$ ( $T=0\text{K}$ )

A variational approach using HNC (\*)

$$\Psi = \prod_{i,j} f_2(r_{ij}) \prod_{i,j,k} f_3(r_{ij}, r_{ik}, r_{jk})$$

$\uparrow$  Jastrow
 $\nwarrow$  Triplets

look at the OBDM

$$\rho(r_{11}) = N \int d^3r_2 \dots d^3r_N \Psi(r_{1-N}) \Psi(r_{1-N}) / \int d^3r |\Psi|^2$$

and the MD

$$\underline{n_{\vec{k}}} = \text{F.T.}(\rho) = \frac{N n_0}{\hbar^3} \delta_{\vec{k},0} + \int d^3r [\rho(r) - \rho_0] e^{i\vec{k}\cdot\vec{r}}$$

$\uparrow$  Condensate fraction
 $\rho_0 = \rho(r \rightarrow \infty) \rightarrow$  LRO

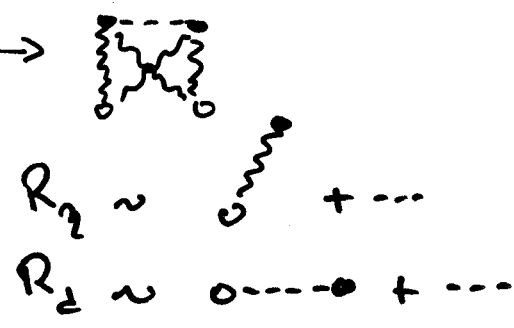
- q) How do you do HNC for EBDM?  $\underline{h(r)} = f^2 - 1$   $0 \dots 0$
- e) Perform cluster expansion with  $\underline{\eta(r)} = f - 1$  ortho points  $\uparrow$  and  $\downarrow$  may be reached only by  $\eta$  correlations



$$\rho(r) = \rho_0 n_0 e^{N_{\eta\eta} + E_{\eta\eta}}$$

$$n_0 = e^{2R_2 - R_1}$$

$N_{\eta\eta}$  from HNC eqs.



(\*) Do you remember Arthur?

An approx. for the element. diagrams

$$g(r) = f^2(r) \exp [N(r) + E(r)]$$

$$\text{HNC/O} \Rightarrow E = 0$$

poor in dense systems

$$\text{HNC/4} \Rightarrow E(r) \cong E_4(r)$$



$$\text{HNC/u} \Rightarrow E(r) \cong E_u(r)$$

Sum of the u-point elem.

Scaling approx.  $\Rightarrow E(r) \cong s E_4(r)$

$\uparrow$  scaling parameter

Fix s by some consistency condition ( $E_{PB} = E_{jF}$ )

IT WORKS !!!

$s \approx 2.7$  for Mettlen

With triplets and for OBDH you have more classes of E-diagrams  $\Rightarrow$  more scalings

$s_T, s_\eta \dots$

HNC/s  $\rightarrow$  HNC/sT extend HNC to triplet correlations

$$g_T(r) = f^2(r) \exp [N(r) + C(r) + E(r)]$$

$$C(r_{12}) = \rho \int d^3r_3 [f_3^2(r_{3,2}) - 1] g_3(r_{1,3,2})$$





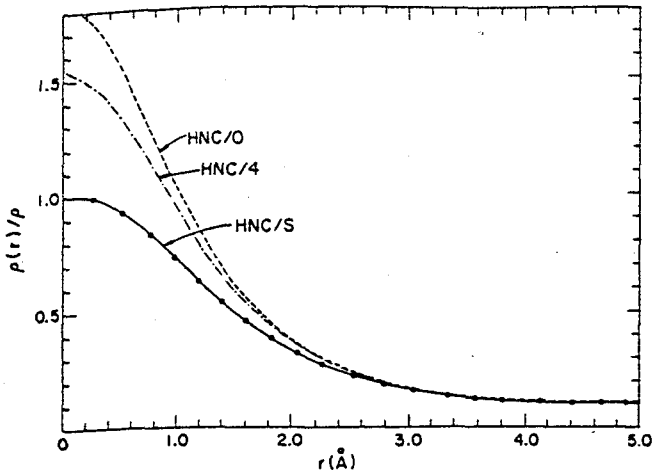


FIG. 3.  $\rho(r_{11'})$  for McMillan-Jastrow wave function at  $\rho=0.365\sigma^{-3}$  in HNC, HNC/4, and HNC/S approximations. The dots give results of Monte Carlo calculations.

elementary diagrams are quite accurate.

The values of the three scaling factors for the McMillan-Jastrow wave function at equilibrium density are found to be

$$s_{dd}=2.72, \quad s_{wd}=1.71, \quad s_{ww}=1.86, \quad (2.23)$$

Puoskari and Kallio<sup>12</sup> use both the two-component mixture and Fantoni's formalism used here to calculate the  $\rho(r_{11'})$ . At any level of approximation the mixture formalism and Fantoni's  $\rho(r_{11'})$  are proportional to each other. The only difference is that in mixture formalism the  $n_0$  is calculated by using the normalization condition (2.20) in Eq. (2.5), whereas Fantoni calculates it independently by Eq. (2.9). PK also use scaling constants  $s_{dd}$ ,  $s_{dw}$ , and  $s_{ww}$  (their  $\kappa_{\alpha\beta}$  equal  $1+s_{\alpha\beta}$  in our notation), and determine them from  $T_{JF}=T_{PB}$ ,  $T_{MD}=T_{JF}$ , and  $T_{MD}(\text{mixture})=T_{MD}$  where  $T_{MD}(\text{mixture})$  is the kinetic energy obtained with  $n(k)$  from mixture formalism. This procedure is identical to ours because  $n(k)(\text{mixture})$  is proportional to  $n(k)$ , and so  $T_{MD}(\text{mixture})=T_{MD}$  is identical to the normalization condition. Thus we do not find that the mixture formalism offers any simplification. PK neglect the contribution of one-body elementary diagrams  $E_d$  and  $E_w$ ; we include them, but find that they are small.

### III. THREE-BODY CORRELATIONS

A significant improvement in the variational energy of liquid helium is obtained by including three-body correlations in the wave function.<sup>7,15</sup> The wave function (the J + T denotes Jastrow plus triplet) is taken as

$$\Psi_{J+T} = \prod_{i < j} f(r_{ij}) \prod_{i < j < k} f_3(r_{ij}, r_{ik}), \quad (3.1)$$

$$f_3(r_{ij}, r_{ik}) = \exp \left[ -\frac{1}{2} \sum_{\text{cyc}} \sum_{l=0,2} \xi_l(r_{ij}) \xi_l(r_{ik}) P_l(r_{ij}, r_{ik}) \right]. \quad (3.2)$$

The  $l=1$  term of  $f_3$  gives the dominant contribution, the  $l=0$  term gives a small contribution, and the  $l=2$  term has negligible effect.<sup>7</sup>

HNC equations for the distribution functions of the J + T wave function have been discussed in Ref. 7. The HNC equations for the density matrix are obtained in an analogous way by replacing the  $E_{xy,xy=dd, wd, \text{ and } ww}$  as follows:

$$E_{xy} = C_{xy} + E_{xy}^g + E_{xy}^t. \quad (3.3)$$

Here  $C_{xy}$  are three-body elements given by

$$C_{dd}(r_{ij}) = \rho \int [f_3^2(r_{ia}, r_{ja}) - 1] \times g_{dd}(r_{ia}) g_{dd}(r_{ja}) d^3 r_a, \quad (3.4)$$

$$C_{wd}(r_{ij}) = \rho \int [f_3(r_{ia}, r_{ja}) - 1] \times g_{wd}(r_{ia}) g_{dd}(r_{ja}) d^3 r_a, \quad (3.5)$$

$$C_{ww}(r_{ij}) = 0. \quad (3.6)$$

$E_{xy}^g$  is the sum of elementary diagrams having only  $g_{xy}-1$  bonds, and  $E_{xy}^t$  is the sum of elementary diagrams having one or more three-body correlations. The  $E_{dd,4}^t$  diagrams are given in Fig. 1 of Ref. 7, and  $E_{wd,4}^t$ ,  $E_{ww,4}^t$ , and  $E_{w,4}^t$  diagrams are given in Figs. 4, 5, and 6, respectively. In these diagrams a wiggly line triangle  $ijk$  with  $l$  as an external point represents

$$[f_3(r_{ij}, r_{ik}) - 1] g_{wd}(r_{ij}) g_{wd}(r_{ik}) g_{dd}(r_{jk}),$$

whereas a plain triangle  $ijk$  represents

$$[f_3^2(r_{ij}, r_{ik}) - 1] g_{dd}(r_{ij}) g_{dd}(r_{ik}) g_{dd}(r_{jk}).$$

As in Ref. 7, a cross on a side  $ij$  of the triangle indicates

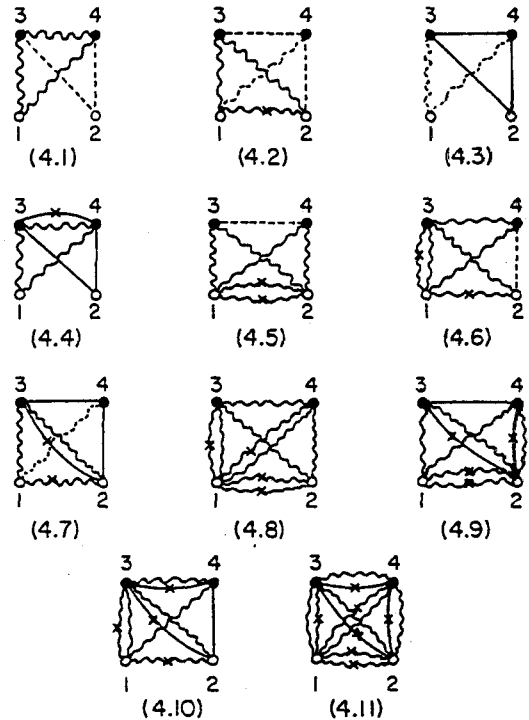


FIG. 4. Four-point  $E_{wd}^t$  diagrams.

TABLE II.  $kn(k)$  with the J + T wave function at various densities.

$k$ ( $\text{\AA}^{-1}$ )	$\rho$ ( $\sigma^{-3}$ )	0.365	0.401	0.438
0.05		0.0167	0.0136	0.0106
0.25		0.0318	0.0264	0.0208
0.45		0.0416	0.0349	0.0279
0.65		0.0458	0.0391	0.0318
0.85		0.0455	0.0398	0.0331
1.05		0.0417	0.0377	0.0324
1.25		0.0350	0.0332	0.0298
1.45		0.0264	0.0266	0.0253
1.65		0.0175	0.0190	0.0196
1.85		0.0112	0.0129	0.0144
2.05		0.0091	0.0105	0.0117
2.25		0.0084	0.0097	0.0109
2.45		0.0066	0.0080	0.0094
2.65		0.0045	0.0058	0.0072
2.85		0.0029	0.0041	0.0054
3.05		0.0019	0.0027	0.0039
3.25		0.0012	0.0018	0.0027
3.35		0.0007	0.0011	0.0019

In general we find that the triplet correlation by itself has little effect on the  $n(k)$ . The  $n(k)$  is seen to decrease exponentially for  $k > 3 \text{ \AA}^{-1}$  in Fig. 7.

The  $kn(k)$  obtained from the neutron scattering data<sup>3,18</sup> is compared with theoretical results in Fig. 8. Both the experimental and the GFMC  $n(k)$  do not have the correct  $k \rightarrow 0$  asymptotic behavior. The difference between GFMC and J + T results has to be attributed to (i) the approximations in the use of J + T wave function, and those in the HNC/S calculation; and (ii) the finite box size

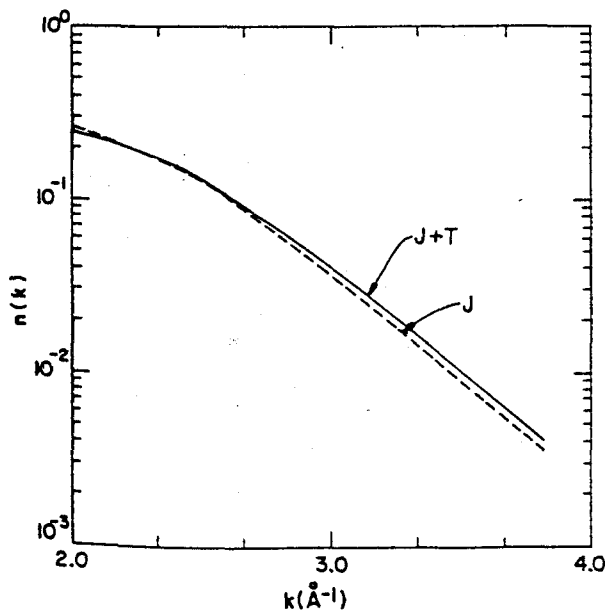


FIG. 7.  $n(k > 2 \text{ \AA}^{-1})$  of the J and J + T wave functions at  $\rho = 0.365\sigma^{-3}$  on log scale. Here  $n(k)$  is normalized according to Eq. (2.19).

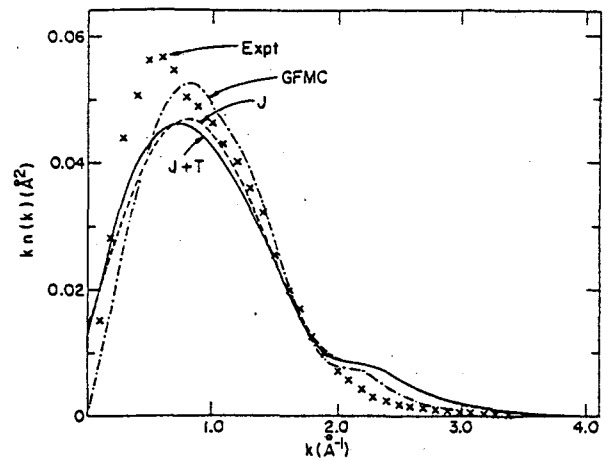


FIG. 8.  $n(k)$  is normalized according to Eq. (4.6). The dashed and solid curves are the results of the present calculation with the Jastrow (J) and Jastrow + triplet (J + T) wave function, respectively. The dashed-dotted curve gives GFMC results from Ref. 17. The experimental data (Refs. 3 and 18) are shown with the crosses.

in the GFMC simulation. The latter effect is particularly manifested at small  $k$ . The difference between theory and experiment may be mostly due to the inadequacy of the Aziz potential, or the impulse approximation used in relating the  $n(k)$  to neutron scattering cross sections at large momentum transfer. The use of impulse approximation for analysis of scattering from hard core liquids has been recently criticized.<sup>19</sup> There certainly is more

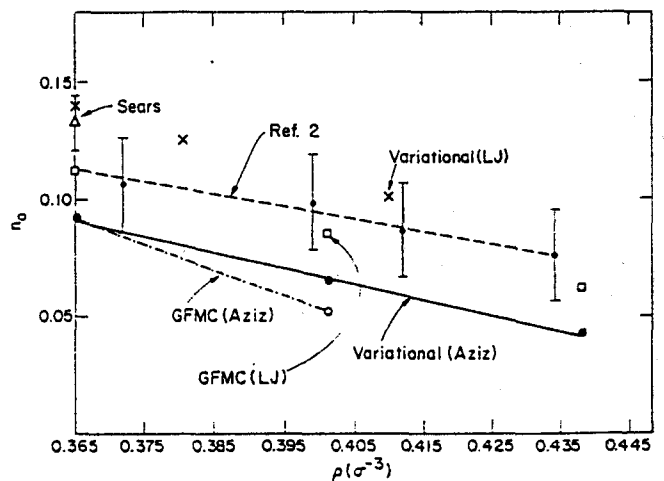


FIG. 9. Comparison of the theoretical and experimental condensate fraction. The solid curve shows the results of this work with Aziz potential. The open circles, joint by a dashed-dotted line, are the results of GFMC calculation with Aziz potential (Ref. 17). GFMC results with Lennard-Jones (LJ) potential are shown with open squares (Ref. 22). The crosses represent the results of Puoskari and Kallio (Ref. 12) variational calculation using LJ potential. The solid circles with the error bars show the data taken from Ref. 2. The dashed line is a guide to the eye. The triangle gives the experimental result at the equilibrium density of Ref. 3.

TABLE III. Results with optimized J and optimized J + T wave functions.

$\rho$ ( $\sigma^{-3}$ )	$s_{dd}$	$s_{ud}$	$s_{uu}$	J	Condensate fraction			Kinetic energy (K)	
					J + T	GFMC	$T_{MD}(J + T)$	$T_{JF}(J + T)$	
0.365	2.44	2.24	2.404	0.098	0.092	0.092	14.86	14.72	
0.401	2.78	2.780	2.916	0.071	0.065	0.052	18.17	17.45	
0.438	3.12	3.120	3.280	0.048	0.043		22.99	20.53	

than qualitative agreement between theory and experiment, marred by significant differences at  $k=0.5$  and  $2.3 \text{ \AA}^{-1}$ . The density dependence of the J + T  $n(k)$  is given in Table II. The  $n(k)$  becomes broader as the density is increased.

The condensate fraction and the kinetic energies are given along with the scaling constants, in Table III. At  $\rho=0.438\sigma^{-3}$  the  $T_{MD}$  is  $\sim 10\%$  larger than the  $T_{JF}$  indicating increased importance of the neglected  $E_{xy}^i$  diagrams.

The theoretical and experimental condensate fractions are compared in Fig. 9. At equilibrium density and GFMC and J + T values of  $n_0$  are identical, but they are  $\sim 20\%$  below the values deduced from neutron scattering

experiments. The density dependence of the J + T  $n_0$  is in crude agreement with that of Ref. 2. On the other hand the experiments of Wirth *et al.*<sup>20</sup> have shown no density dependence of  $n_0$ , while Mook<sup>21</sup> finds a much stronger decrease in  $n_0$  with  $\rho$ .

#### ACKNOWLEDGMENTS

The authors wish to thank Dr. R. O. Hilleke, Dr. R. M. Panoff, Dr. D. L. Price, Dr. V. F. Sears, Dr. R. O. Simmons, Dr. P. E. Sokol, and Dr. P. A. Whitlock for communicating their results. This work was supported by the U.S. Department of Energy, Division of Materials Sciences, under Contract No. DE-AC02-76ER01198.

\*Present address: Department of Physics, Aligarh Muslim University, Aligarh 202001, India.

<sup>1</sup>F. London, *Nature* (London) **141**, 643 (1938); *Phys. Rev.* **54**, 947 (1938).

<sup>2</sup>P. E. Sokol, R. O. Simmons, R. O. Hilleke, and D. L. Price (unpublished).

<sup>3</sup>V. F. Sears, *Phys. Rev. B* **28**, 5109 (1983).

<sup>4</sup>V. F. Sears, E. C. Svensson, P. Martel, and A. D. B. Woods, *Phys. Rev. Lett.* **49**, 279 (1982); V. F. Sears and E. C. Svensson, *Phys. Rev. Lett.* **43**, 2009 (1979); A. D. B. Woods and V. F. Sears, *Phys. Rev. Lett.* **39**, 415 (1977).

<sup>5</sup>M. H. Kalos, M. A. Lee, P. A. Whitlock, and G. V. Chester, *Phys. Rev. B* **24**, 115 (1981).

<sup>6</sup>R. A. Aziz, V. P. S. Nain, J. S. Carley, W. L. Taylor, and G. T. McConville, *J. Chem. Phys.* **70**, 4330 (1979).

<sup>7</sup>Q. N. Usmani, S. Fantoni, and V. R. Pandharipande, *Phys. Rev. B* **26**, 6123 (1982).

<sup>8</sup>S. Fantoni, *Nuovo Cimento A* **44**, 191 (1978).

<sup>9</sup>M. L. Ristig, P. M. Lam, and J. W. Clark, *Phys. Lett.* **55A**, 101 (1975); P. M. Lam and M. L. Ristig, *Phys. Rev. B* **20**, 1960

(1979).

<sup>10</sup>A. Fabrocini and S. Rosati, *Nuovo Cimento D* **1**, 615 (1982).

<sup>11</sup>Q. N. Usmani, B. Friedman, and V. R. Pandharipande, *Phys. Rev. B* **25**, 4502 (1982).

<sup>12</sup>M. Puoskari and A. Kallio, *Phys. Rev. B* **30**, 152 (1984).

<sup>13</sup>Daniel Shiff and Loup Verlet, *Phys. Rev.* **160**, 208 (1967).

<sup>14</sup>M. H. Kalos, D. Levesque, and L. Verlet, *Phys. Rev. A* **9**, 2178 (1974).

<sup>15</sup>K. Schmidt, M. H. Kalos, M. A. Lee, and G. V. Chester, *Phys. Rev. Lett.* **45**, 573 (1980).

<sup>16</sup>L. Reatto and G. V. Chester, *Phys. Lett.* **22**, 276 (1966).

<sup>17</sup>P. A. Whitlock and R. M. Panoff (unpublished).

<sup>18</sup>V. F. Sears (private communication).

<sup>19</sup>J. J. Weinstein and J. W. Negele, *Phys. Rev. Lett.* **49**, 1016 (1982).

<sup>20</sup>F. W. Wirth, D. A. Ewen, and R. B. Hallock, *Phys. Rev. B* **7**, 5530 (1983).

<sup>21</sup>H. A. Mook, *Phys. Rev. Lett.* **51**, 1454 (1983).

<sup>22</sup>P. A. Whitlock, D. A. Ceperely, G. V. Chester, and M. H. Kalos, *Phys. Rev. B* **19**, 5598 (1979).

# BEC in $^4\text{He}$ clusters

Correlated w.f. with  $f_2$  and  $f_3$

$$\psi(N) = \pi f_2 \pi f_3 \pi f_1$$

Continuing 3-body correlation  
(Solution of a WS well or  
w Fermi function)

Use VME (Pendharpande, Pieper, Wiringa) or  
MNE (Krot, deck.) to compute the finite droplets  
OBDM

In inhom. Bose system with OBD  $\rho(\vec{r})$

a) in MEAN FIELD all particles condense in  
 $\phi_0(\vec{r}) = [\rho(\vec{r})/N]^{1/2}$

b) actually

$n_0$  condense in the NATURAL  
ORBIT  $\psi_0(\vec{r})$  (diagonalizing  
the OBDM)

$$\rho(\vec{r}_1, \vec{r}_1) = \sum_i n_i \psi_i^*(\vec{r}_1) \psi_i(\vec{r}_1)$$

$$\rho(\vec{r}) = \sum_i n_i |\psi_i(\vec{r})|^2 \quad \leftarrow \text{OBDM}$$

$$\text{MD} \rightarrow n_{\vec{k}} = \sum_i n_i |\hat{\psi}_i(\vec{k})|^2$$

$$\hat{\psi}_i(\vec{k}) = \text{F.T.}(\psi_i)$$

$$\rho_c(\vec{r}) = n_0 |\psi_{1s}(\vec{r})|^2$$

$$\psi_{1s}(\vec{r}) \approx N [1 - \alpha \rho(\vec{r})/\rho_0] \phi_{1s}(\vec{r}) = N [1 - \alpha \rho(\vec{r})/\rho_0] \sqrt{\frac{\rho(\vec{r})}{N}}$$

$$\Rightarrow n_0^{1/2} [\rho(\vec{r})] = N [1 - \alpha \rho(\vec{r})/\rho_0] \quad \alpha = .68 \quad N=70$$

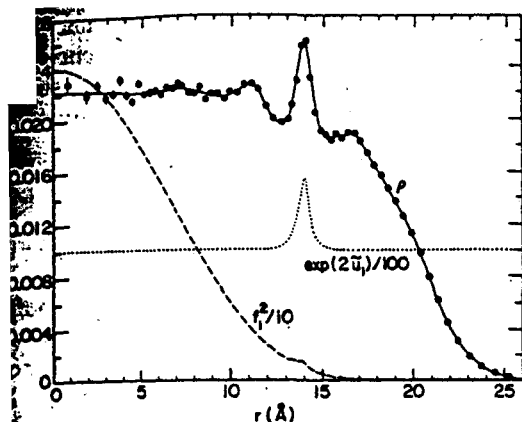


FIG. 8. Density distribution for the 728-atom  ${}^4\text{He}$  drop with a sharp peak near the surface. The dashed curve is the single-particle density divided by 10. The dotted curve is  $\exp(2\bar{u}_1)$  divided by 100.

than that of the liquid.

The unit radii  $r_0(N)$  are defined as

$$r_0(N) = \left[ \frac{2}{3} \langle r^2(N) \rangle \right]^{1/2} / N^{1/3}, \quad (5.5)$$

where  $\langle r^2(N) \rangle$  is the mean-square radius of an  $N$ -body drop. The values of  $r_0(N)$  for both  ${}^4\text{He}$  and  ${}^3\text{He}$  drops are given in Table XIV. The rms radii of the drops have negligible statistical uncertainty resulting from Monte Carlo sampling. The main error in  $\langle r^2(N) \rangle$  comes from the uncertainty in choosing the best variational wave functions. In particular, the uncertainty in the radius of the  $N=20$   ${}^3\text{He}$  (metastable) drop is large because the energy does not change significantly with a  $\pm 10\%$  variation in radius. The energies of larger drops are much more sensitive to their radii, and thus their radii are much better determined.

The unit radius  $r_0(\infty)$  of the liquid can be extracted by fitting the  $r_0(N)$  by a polynomial in  $N^{-1/3}$ . A fit to the calculated unit radii of  $N=40-728$   ${}^4\text{He}$  drops with a third-order polynomial gives  $r_0(\infty) = 2.21(4)$  Å for  ${}^4\text{He}$ , in good agreement with the experimental value of 2.2 Å as well as with the GFMC value for the Aziz potential. The quoted error of  $r_0(\infty)$  is an estimate based on both the variational and extrapolation errors. Fits to the radii of  ${}^3\text{He}$  drops having  $N=40-240$  give  $r_0(\infty) = 2.5(1)$  in agreement with the experimental value of 2.5 Å. We note that the central densities of  $N=240$   ${}^4\text{He}$  drops (Fig. 2) and  $N=240$   ${}^3\text{He}$  drop (Fig. 3) are compatible with these values of  $r_0(\infty)$ .

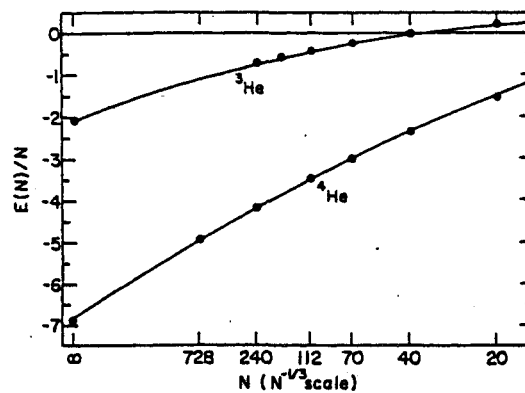


FIG. 9.  $E/N$  for the  ${}^3\text{He}$  and  ${}^4\text{He}$  drops. The abscissa is  $N$  on an  $N^{-1/3}$  scale. The curves are from rows 2 and 3 of Table XIII.

## VI. DISCUSSION

We have made VMC calculations of the ground states of small- to moderate-sized drops of liquid  ${}^4\text{He}$  and  ${}^3\text{He}$ . Comparisons with GFMC calculations show that our binding energies are typically 0.1 K per atom too low. There is unfortunately no suitable experimental data to which these calculations can be compared. A mass spectrometer experiment<sup>33</sup> has reported the observation of magic numbers for both  ${}^4\text{He}$  and  ${}^3\text{He}$  drops and also  ${}^3\text{He}$  drops containing as few as four atoms. However, the drops are charged and may be fragmented in the mass spectrometer. Detailed GFMC calculations<sup>34</sup> for neutral  ${}^4\text{He}$  drops show only a smooth energy versus drop-size relation. The very small binding energy for eight  ${}^4\text{He}$  atoms with Fermi statistics obtained with GFMC makes it certain that eight  ${}^3\text{He}$  atoms are not bound. For these reasons, we agree with the conclusions of Ref. 34, that the charge on the drops has significantly altered their properties. Macroscopic liquid drops having more than 10000 helium atoms have been used in experiments.<sup>35</sup> Experimental studies of small neutral drops would be very interesting. In particular, there is the question of what is the smallest number of  ${}^3\text{He}$  atoms that will form a bound state. Our calculations suggest that this number is just slightly less than 40. However, if our energy for 40  ${}^3\text{He}$  atoms is 0.1 K too high, the number will be close to 30.

There is an interesting contrast between studies of liquid-helium drops and nuclei. By fitting liquid-drop expansions to the drop energies, we can obtain binding-

TABLE XIII. Liquid-drop energy fits. The coefficients of the polynomial defined in Eq. (5.1) are given. The last column gives  $\chi^2$  per degree of freedom.

System	Range	$E_0$	$E_1$	$E_2$	$\chi^2/N_f$
${}^4\text{He}$	$N=20-728$	-7.00	19.6	-13.3	9.0
${}^4\text{He}$	$N=40-728$	-6.85	18.2	-9.9	2.0
${}^3\text{He}$	$N=20-240$	-2.09	9.9	-9.9	2.9
${}^3\text{He}$	$N=40-240$	-1.90	8.3	-6.4	0.36
${}^3\text{He}$	$N=70-240$	-2.09	10.0	-10.5	0.04

This method has the advantage of introducing no bias about the functional form of  $u_{nl}(r)$  but has the disadvantage, due to the relatively large sampling errors in  $\rho_l(r, r')$  for small  $r$  or  $r'$ , of not producing radial functions with the correct  $r'^{l+1}$  behavior at the origin. The statistical errors in the so-extracted  $u_{nl}(r)$  also make it difficult to compute the Fourier transforms  $\bar{u}_{nl}(k)$ .

In the second method we expand the  $\rho_l(r, r')$  in terms of the oscillator functions  $h_{nl}(r)$ :

$$M_{ij}^l = \int \int h_{il}(r) \rho_l(r, r') h_{jl}(r') dr dr' \quad (3.9)$$

for  $i, j \leq I$  with  $I$  less than the number of points on the grid used to compute  $\rho_l(r, r')$ . The eigenvectors of  $M^l$  may be used to construct  $u_{nl}(r)$  with the correct behavior at the origin.

Table I shows the eigenvalues of  $\rho_{l=0}(r, r')$  for the 70-atom  ${}^3\text{He}$  drop computed by these methods. (Note that the eigenvalues are twice the occupation numbers.) We used a 28-element grid to compute  $\rho_l(r, r')$  so method 1 gives us 28 eigenvalues. However, because of the statistical errors in  $\rho_0(r, r')$ , eleven of these are negative (the sum of the negative eigenvalues is  $-0.01$ ). Column 4 of Table I shows the ten largest eigenvalues. Columns 1 to 3 show the corresponding eigenvalues computed using 11, 16, and 21 oscillator functions, respectively. The first, third, and fifth eigenvectors computed by method 1 (symbols) and with 11 and 16 oscillator functions (curves) are shown in Fig. 3. The curves for 21 oscillator functions are indistinguishable from those for 16 functions. It can be seen that the two methods are in good agreement and that eigenvalues down to  $\sim 0.01$  are probably reliable. In the rest of the paper we present results obtained using 16 oscillator functions.

### B. Natural orbitals of the $N = 70$ Liquid ${}^4\text{He}$ Drop

Some of the  $s$ -wave natural orbitals of the 70-particle Bose-liquid  ${}^4\text{He}$  drop are shown in Fig. 4 along with the  $1s$  mean-field orbital. We note that all the natural orbit-

TABLE I. Eigenvalues of  $\rho_{l=0}(r, r')$  for 70  ${}^3\text{He}$  atoms. Columns 1-3 show the eigenvalues computed in an oscillator basis containing, respectively, the first 11, 16, and 21 oscillator functions. The last column shows the eigenvalues resulting from a direct diagonalization of  $\rho_{l=0}(r, r')$  on a  $28 \times 28$  point grid in  $r$  space. In all cases only the first ten eigenvalues are shown.

$n$	$I=11$	$I=16$	$I=21$	$28 \times 28$
1	1.0801	1.0803	1.0804	1.0816
2	1.2565	1.2575	1.2580	1.2600
3	1.6963	1.6987	1.6996	1.7066
4	0.1476	0.1477	0.1477	0.1495
5	0.0782	0.0784	0.0784	0.0799
6	0.0376	0.0378	0.0382	0.0427
7	0.0160	0.0197	0.0197	0.0232
8	0.0007	0.0065	0.0067	0.0084
9	$4.0 \times 10^{-5}$	0.0010	0.0022	0.0071
10	$-1.0 \times 10^{-6}$	0.0004	0.0010	0.0044

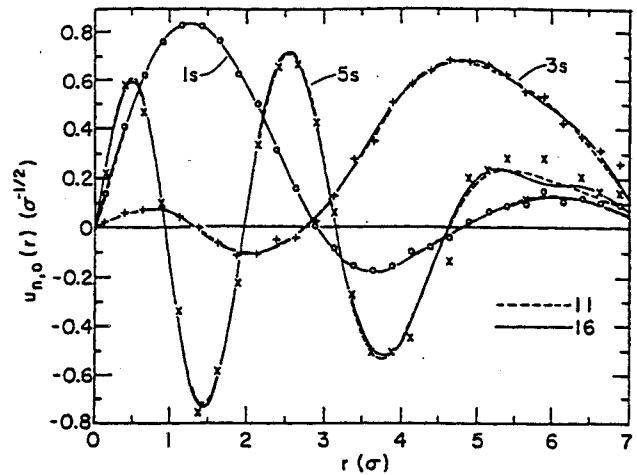


FIG. 3. The  $1s$ ,  $3s$ , and  $5s$  natural orbitals of the 70-atom  ${}^3\text{He}$  drop obtained with 11 (dashed curves) and 16 (solid curves) oscillator functions. The symbols show the eigenfunctions obtained by diagonalizing in coordinate space.

als are confined in the region where  $\rho(r) \neq 0$ . Equation (1.7) implies that the  $\psi_i(r)$  are zero where  $\rho(r) = 0$ . The occupation numbers of the natural orbitals are given in Table II. A significant fraction (36%) of the particles are condensed in the  $1s$  natural orbital of the 70-particle drop, as against  $\sim 10\%$  in the extended liquid. The dependence of the condensate fraction on the number of particles is discussed in Sec. IV.

The partial density of the particles condensed in the  $1s$  natural orbital is called the condensate density,

$$\rho_c(r) = n_{1s} |\psi_{1s}(r)|^2, \quad (3.10)$$

and it is compared with the total density  $\rho(r)$  in Fig. 5. We note that at the center of the drop  $\rho_c(0) \approx 0.1\rho(0)$ , as expected from studies of the extended liquid.

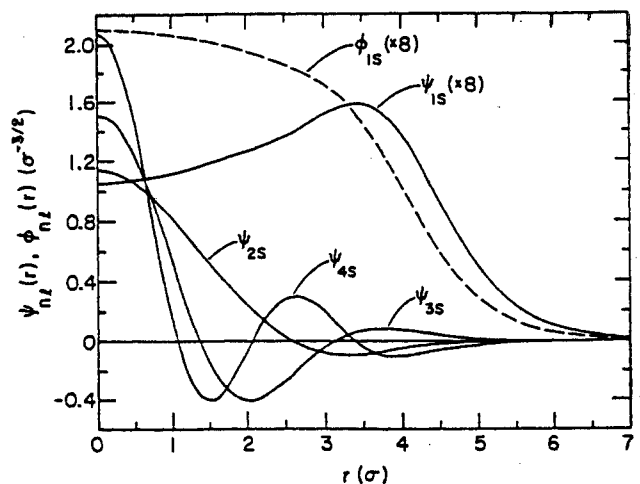


FIG. 4. The  $s$ -wave natural orbitals ( $1s$  to  $4s$ ) of the 70-particle Bose-liquid  ${}^4\text{He}$  drop (solid lines). The dashed curve shows the  $1s$  mean-field orbital. The  $\psi_{1s}$  and  $\phi_{1s}$  have been multiplied by 8.

TABLE II. Occupation numbers of natural orbitals of the  $N=70$  Bose-liquid  ${}^4\text{He}$  drop.

$n, l$	$n_{n,l}$	$n, l$	$n_{n,l}$	$n, l$	$n_{n,l}$
1s	25.33	1h	0.24	1k	0.104
1p	0.49	2f	0.22	2i	0.086
1d	0.44	3p	0.22	3g	0.078
2s	0.44	1i	0.19	4d	0.077
1f	0.37	2g	0.17	5s	0.100
2p	0.35	3d	0.16	1l	0.063
1g	0.30	4s	0.19	2j	0.060
2d	0.28	1j	0.14	3h	0.046
3s	0.30	2h	0.12	4f	0.049
		3f	0.11	5p	0.046
		4p	0.11		

In Bose-liquid drops the 1s natural orbital can be well approximated as follows:

$$\begin{aligned} \psi_{1s}(r) &\approx A[1-0.68\rho(r)/\rho_0]\phi_{1s}(r) \\ &\approx A[1-0.68\rho(r)/\rho_0]\sqrt{\rho(r)/N}, \end{aligned} \quad (3.11)$$

where  $A$  is a normalization constant and  $\rho_0$  is the equilibrium density of liquid  ${}^4\text{He}$  ( $0.365\sigma^{-3}$ ). The wave function obtained from this approximation is practically indistinguishable from the  $\psi_{1s}(r)$  in Fig. 4. The factor multiplying  $\sqrt{\rho(r)/N}$  in Eq. (3.11) can be interpreted as  $\sqrt{n_0[\rho(r)]}$ , where  $n_0(\rho)$  is the condensate fraction in liquid  ${}^4\text{He}$  at density  $\rho$ , from the argument given in the next paragraph. Since extended liquid at  $\rho < \rho_0$  is unstable, only  $n_0(\rho)$  for  $\rho \geq \rho_0$  has been studied.<sup>4</sup> In Fig. 6 we show that the function  $(1-0.68\rho/\rho_0)$  provides a continuation of  $\sqrt{n_0(\rho)}$  for  $\rho < \rho_0$ .

Consider an inhomogeneous Bose system with a densi-

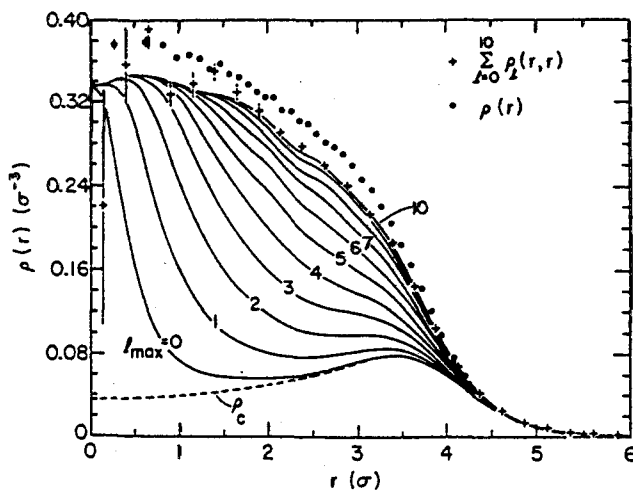


FIG. 5. The density  $\rho(r)$  of the 70-atom  ${}^4\text{He}$  drop (dots with error bars) from Ref. 1. The curves show the cumulative contributions of the natural orbitals up to a given  $l_{\max}$  as obtained from the oscillator expansions. The crosses and error bars show the sum of  $\rho_l(r, r)$  for  $l$  up to 10 and are to be compared with the uppermost curve. The dashed curve is the condensate contribution  $\rho_c(r)$ .

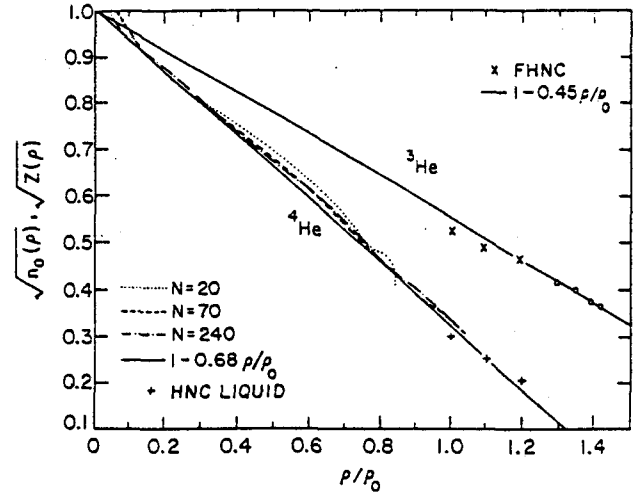


FIG. 6. Condensate amplitudes  $\sqrt{n_0}$  as a function of density for liquid  ${}^4\text{He}$  (lower curves and symbols) and the  $\sqrt{Z(\rho)}$  for liquid  ${}^3\text{He}$  (upper line and symbols). The solid lines are the approximations  $n_0(\rho) = (1-0.68\rho/\rho_0)^2$  ( ${}^4\text{He}$ ) and  $Z(\rho) = (1-0.45\rho/\rho_0)^2$  ( ${}^3\text{He}$ ). The plus signs are from Ref. 4, the  $\times$ 's are from Ref. 5, and the circles are obtained by assuming that the experimental effective mass (Ref. 8) is given by  $0.8/Z$  (Ref. 5). The ratio  $\chi_{1s}(r)/\sqrt{\rho(r)}$ , as described in the text, is shown for the 20-atom (dotted), 70-atom (dashed), and 240-atom (dot-dash)  ${}^4\text{He}$  drops.

ty distribution  $\rho(r)$ . In mean-field theory, all the particles occupy the state  $\phi_0(r) = \sqrt{\rho(r)/N}$ . In reality, a certain fraction of the particles are condensed in the natural orbital  $\psi_0(r)$ . Now let us pretend that the inhomogeneous system is a large tank of liquid  ${}^4\text{He}$ , with an external potential applied to the  $x > 0$  half such that the density distribution of the liquid in this tank is given by

$$\rho(r) = \begin{cases} \rho_L, & x \ll 0 \\ \rho_R, & x \gg 0. \end{cases} \quad (3.12)$$

$$(3.13)$$

Now the density of particles having momenta  $k \sim 0$  at  $x \ll 0$  is given by  $n_0(\rho_L)\rho_L$ , while for that at  $x \gg 0$  it is  $n_0(\rho_R)\rho_R$ . Thus we have

$$N_c \psi_0^2(r) = \begin{cases} n_0(\rho_L)\rho_L, & x \ll 0 \\ n_0(\rho_R)\rho_R, & x \gg 0, \end{cases} \quad (3.14)$$

$$(3.15)$$

where  $N_c$  is the number of particles condensed in the natural orbital  $\psi_0$ . This implies that when  $\rho(r)$  is a slowly varying function of  $r$ , the natural orbital  $\psi_0(r)$  is approximately given by

$$\psi_0(r) \approx A \sqrt{n_0[\rho(r)]} \sqrt{\rho(r)/N} = A \sqrt{n_0[\rho(r)]} \phi_0(r). \quad (3.16)$$

Equation (3.16) can be considered as a local-density approximation (LDA) for the condensate natural orbital. It is a good approximation in all the Bose-liquid drops ( $N=20-240$ ) studied in this work.

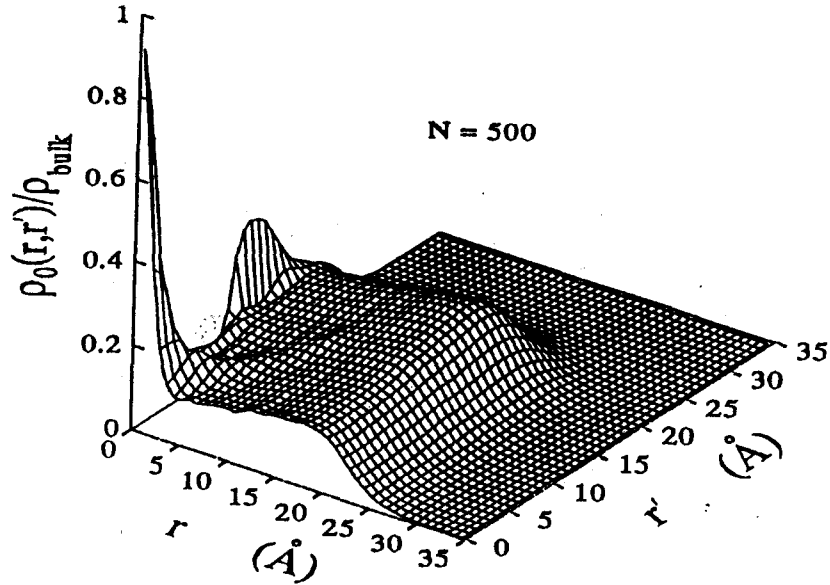


Fig. 13. Same as Fig.10 but for N=500

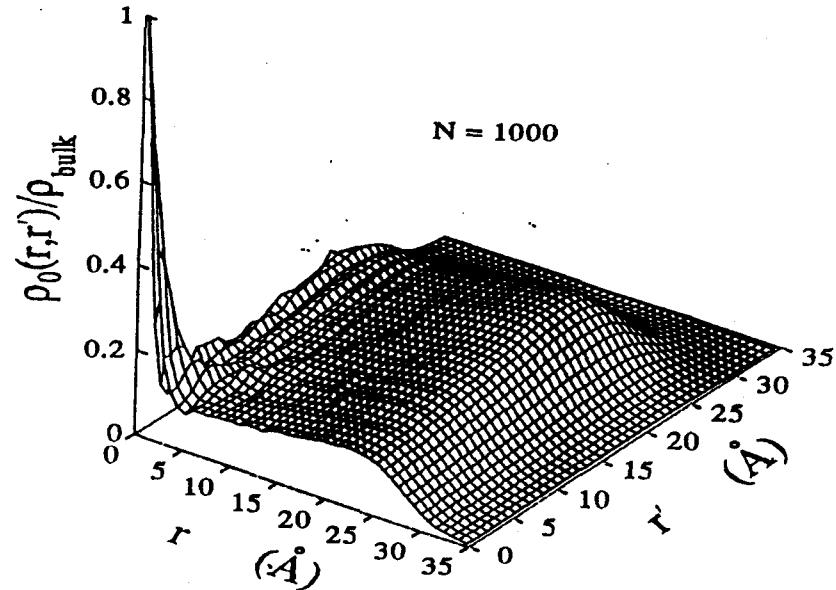


Fig. 14. Same as Fig.10 but for N=1000

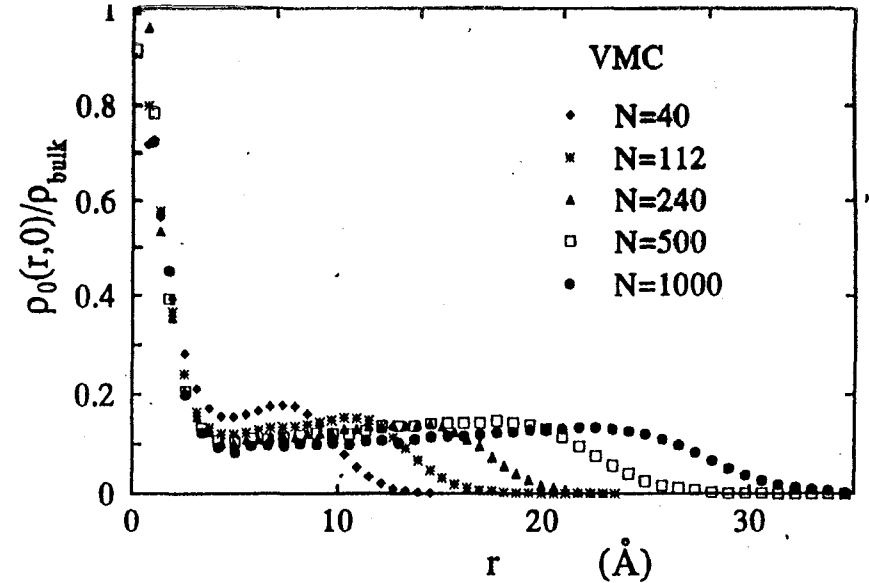


Fig. 15. The variation of the edge of the  $\ell = 0$  density matrix as a function of droplet size.

is asymmetric (only  $r$  is binned), the resulting function is symmetric as it should. (The fish-fin like structures near  $r = 0$  are artifacts due to poor statistics amplified by the small bin size, like that of determining the central density. These should be ignored.) We note that for all droplets: 1)  $\rho_0(r, r')/\rho_{\text{bulk}}$  drops quickly from one to about 0.1 whenever either  $r$  or  $r'$  is greater than 4 Å. 2) Whenever  $r$  or  $r'$  is greater than 4 Å,  $\rho_0(r, r')/\rho_{\text{bulk}}$  is roughly constant, resulting in a plateau-like structure. 3) This plateau extends out to about the droplet radius and grows steadily with increase droplet sizes. 4) The table-top-like sharp corner strongly suggests that  $\rho_0(r, r')$  is a product of two identical functions, i.e.,

$$\rho_0(r, r') \propto \phi(r)\phi(r').$$

Since  $\rho_0(r, r')$  can be expanded in an eigenfunction expansion, the above suggest that it is likely to be dominated by a single term, that of its largest eigenfunction. 5) If this is the case, this largest eigenfunction must be roughly proportional to  $\rho_0(r, 0)/\rho_{\text{bulk}}$ . In Fig.15, we show the latter for all droplet sizes considered. The results are now strikingly similar to the bulk density matrix of Fig.1. This edge function drops from 1 to  $\approx 0.1$  from the center out to about 4 Å. It then remains roughly constant all the way out to the rim of the droplet. (The slight rise is too fine a structure to be trust in a variational calculation.) As  $N$  increases, there is a clear systematic convergence to the bulk condensate value from above. Thus the  $\ell = 0$  component of the one-body density matrix gives an excellent visual characterization of the growth of the condensate in Helium droplets.



# Dilute gas

$$r_0 \sim \left(\frac{3}{4\pi\bar{n}_0}\right)^{1/3} \rightarrow \text{average spacing}$$

$$\bar{n}_0 = \text{average density}$$

$R$  = range of the interaction

$$\Downarrow \boxed{r_0 \gg R}$$

At low energy only binary collisions matter  
 $\rightarrow$  characterized by one parameter

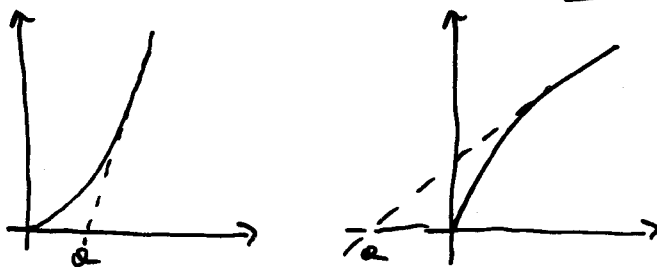
The s-wave scattering length  $\rightarrow \underline{a}$   
 (asymptotic solution of the  $\psi$ -energy Schr. eq.)

$$r\psi_{\text{free}}(r \rightarrow \infty) \sim r - a \quad \delta_0(k) = -ka \quad (k \rightarrow 0)$$

$$-\frac{\hbar^2}{m} \nabla^2 \psi_{\text{free}} = 0$$

$a > 0$   $\rightarrow$  effectively repulsive strong potential

$a < 0$   $\rightarrow$  some effective attraction

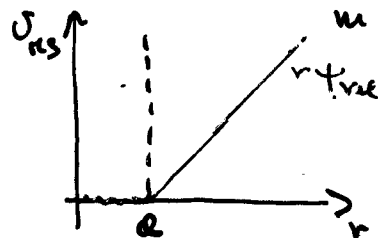


for HF approaches

① point-like pseudopotential

$$V(r) \rightarrow \frac{4\pi\hbar^2}{m} a \delta(r)$$

② HS potential with  $C = a$



$$C_{HS} = a \quad r \leq a$$

$$= 0 \quad r > a$$

Diluteness condition  $\Rightarrow \bar{n}_0 |\alpha|^3 \ll 1$

$\uparrow$  average gas parameter

$$\alpha(^{87}\text{Rb}) = 5.27 \text{ nm}$$

$$\alpha(^7\text{Li}) = -1.45 \text{ nm}$$

$$\bar{n}_0 \sim 10^{13} \div 10^{15} \text{ cm}^{-3} \Rightarrow \bar{n}_0 |\alpha|^3 < 10^{-3}$$

#

Homog. Bose gas of HS - Mean Field (Bogoliubov)

$$\hat{H} = \int d^3r \hat{\psi}^\dagger(\vec{r}) \left[ -\frac{\hbar^2}{2m} \nabla^2 + (U_{\text{ext}}(\vec{r})) \right] \hat{\psi}(\vec{r}) +$$

$$+ \frac{1}{2} \int d^3r \int d^3r' \hat{\psi}^\dagger(\vec{r}) \hat{\psi}^\dagger(\vec{r}') \underbrace{U(|\vec{r}-\vec{r}'|)}_{\uparrow g \delta(\vec{r}-\vec{r}')} \hat{\psi}(\vec{r}) \hat{\psi}(\vec{r}')$$

$\hat{\psi}^\dagger, \hat{\psi} \rightarrow$  boson field operators

$$g \sim \frac{\hbar^2}{m}$$

$$\hat{\psi}(\vec{r}) = \sum_{\alpha} \psi_{\alpha}(\vec{r}) \hat{Q}_{\alpha} = \psi_0 \hat{Q}_0 + \sum_{\alpha \neq 0} \psi_{\alpha}(\vec{r}) \hat{Q}_{\alpha}$$

$\nwarrow$  SP w.f.   
  $\uparrow$  annih. op.

$$\hat{Q}_0 |n_0 - n_{\alpha} \dots\rangle = \sqrt{n_0} |n_0 - n_{\alpha} \dots\rangle$$

$$\hat{Q}_{\alpha}^{\dagger} |n_0 \dots n_{\alpha} \dots\rangle = \sqrt{n_{\alpha} + 1} |n_0 \dots n_{\alpha} + 1 \dots\rangle$$

at BEC  $n_0 \approx N_0 \gg 1$  and  $N_0 \sim N$  ( $N \rightarrow \infty$ )

so  $N_0 \pm 1 \sim N_0$  and  $\hat{Q}_0^{\dagger}, \hat{Q}_0 \rightarrow$  c numbers  $\rightarrow \sqrt{N_0}$

$$\hat{\psi}(\vec{r}) = \sqrt{\frac{N_0}{\Omega}} + \hat{\psi}'(\vec{r}) \quad \text{small perturbation}$$

$$\frac{E^{HS}}{N} = \frac{2\pi\hbar^2 n_s a}{m} \left[ 1 + \frac{128}{15} \frac{(n_s a^3)^{1/2}}{\sqrt{\pi}} + 8 \left( \frac{4\pi}{3} - \sqrt{3} \right) \ln(n_s a^3) + \alpha (n_s a^3)^2 \right]$$

↑ just ord.                      ↑ Sum of ladder diagrams (Lee and Yang)                      ↑ Wu

Low density expansion

$$\frac{E^{HS}}{N} = \left( \frac{E^{HS}}{N} \right)_{LO1} + \left( \frac{E^{HS}}{N} \right)_{LO2} + \dots$$

Hardy - Bose gas of HS - variational

Start from  $H = -\frac{\hbar^2}{2m} \sum_i \nabla_i^2 + \sum_i V_{ext}(r_i) + \sum_{i < j} V(r_{ij})$

↑ HS pot.

Jastrow correlated w.f.  $\Psi(N) = \prod_{i < j} f(r_{ij})$

Compute and minimize  $\frac{E}{N} = \rho \int d^3 r_{12} g(r_{12}) \Psi_f(r_{12})$

Use HNE to evaluate  $g(r)$

SR correlation → minimize two body energy

$$\frac{E^{2b}}{N} = \rho \int d^3 r f^2(r) \Psi_{SR}(r) \text{ with}$$

the boundary condition

$$f(r \geq d) = 1 \quad \dot{f}(r=d) = 0$$

$d = \text{variational}$

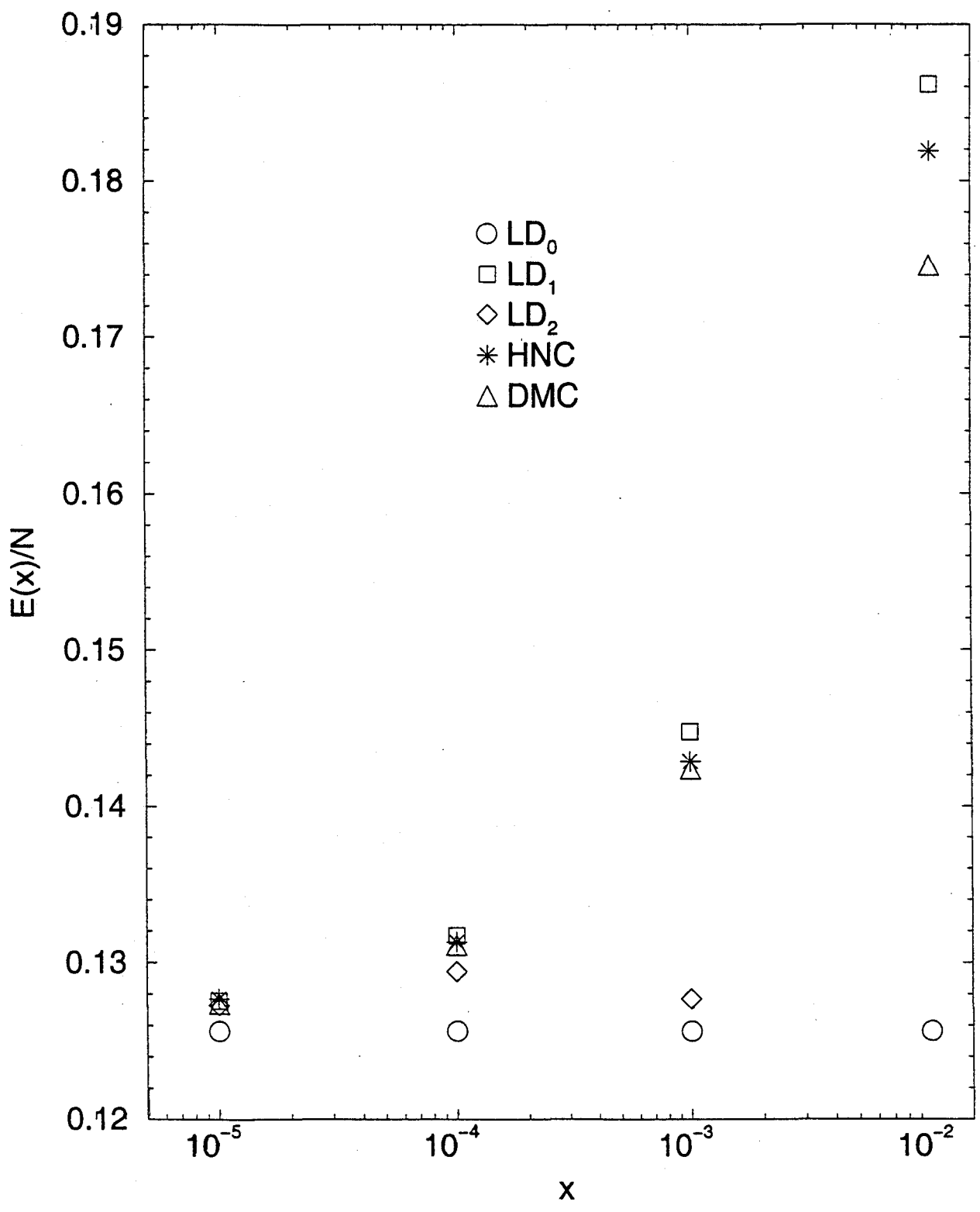
$$f(r) = u(r)/r \quad -u'' = \frac{\hbar^2}{m} \tilde{E} u$$

$$f(r) = \frac{d}{r} \frac{\sin[k(r-d)]}{\sin[k(d-d)]} \text{ with } \text{ctg}[k(d-d)] = \frac{1}{kd}$$

$k^2 = m \tilde{E} / \hbar^2$                        $= 1/kd$

LR correlation  $\rightarrow$  minimize  $\frac{E^{HNC}}{N}$  (ELL equation)

Homog. Bose gas of HS - Benchmark  $\rightarrow$  DMC



Bose gas in a trap (switch on  $V_{\text{ext}}$ )

Mean Field  $\rightarrow \hat{\Psi}(\vec{r}) = \phi(\vec{r}) + \hat{\psi}(\vec{r})$

$\uparrow$  external field (order parameter)  $\rightarrow$   
 $\rightarrow$  Condensate w.f.

$n_0(\vec{r}) = |\phi(\vec{r})|^2$   $\rightarrow$  condensate density

0th ord.  $\rightarrow$  GP energy functional

$$E[\phi] = \int d^3r \left[ \frac{\hbar^2}{2m} \nabla \phi \cdot \nabla \phi + V_{\text{ext}}(\vec{r}) |\phi|^2 + \frac{1}{2} g |\phi|^4 \right] \quad g = \frac{4\pi \hbar^2 a}{m}$$

Minimize  $E_{\text{GP}}$  with respect to  $\phi$   $\rightarrow$

$\rightarrow$  GP equation

$$\left( -\frac{\hbar^2}{2m} \nabla^2 + V_{\text{ext}}(\vec{r}) + g |\phi|^2 \right) \phi(\vec{r}) = \mu \phi(\vec{r})$$

$\uparrow$  Chem. pot.

$$\int d^3r |\phi|^2 = \int d^3r n_0(\vec{r}) = N_0 = N \quad (\text{mean field})$$

from  $i\hbar \frac{\partial}{\partial t} \hat{\Psi} = [\hat{\Psi}, \hat{H}] \rightarrow i\hbar \frac{\partial \phi}{\partial t} = \left( -\frac{\hbar^2}{2m} \nabla^2 + V_{\text{ext}} + g |\phi|^2 \right) \phi$

time dep. GP equation

# Large N limit (Thomas Fermi)

$\frac{2}{18}$

The density becomes flat  $\Rightarrow$  disregard the kinetic energy term in GP

$$\left( \frac{1}{2} m \omega_{ho}^2 r^2 + g \underbrace{|\phi|^2}_{n_0(\vec{r})} \right) \phi = \mu \phi$$

$$\underline{n_0(\vec{r})} = |\phi|^2 = \left[ \mu - \frac{1}{2} m \omega_{ho}^2 r^2 \right] \frac{1}{g}$$

class. turning point  $\mu = \epsilon_{ext}^{cl}$

Condition  $\underline{n_0(\vec{r})} \geq 0 \Rightarrow r^2 \leq R^2 = 2\mu / m\omega_{ho}^2$

Normalize  $\int_0^R n_0(\vec{r}) d^3r = N \Rightarrow \mu = \frac{\hbar \omega_{ho}}{2} \left( \frac{15 N a}{R_{ho}} \right)^{2/5}$

$n_0(\vec{r}), \mu, R = R_{ho} \left( \frac{15 N a}{R_{ho}} \right)^{2/5}$  analytical in TF

$$n_0^{TF}(0) = \mu/g \ll n_0^{ho}(0) = N / (\pi^{3/2} R_{ho}^3)$$

$$\frac{n_0^{TF}(0)}{n_0^{ho}(0)} = \frac{15^{2/5} \pi^{1/2}}{8} \left( \frac{N a}{R_{ho}} \right)^{-2/5}$$

decreases with N

$\frac{N a}{R_{ho}} \sim 10^5 \div 10^7$  for  $^{23}\text{Ne}$  and  $^{87}\text{Rb}$

# Central density reduced by one/two order of magnitudes by atom-atom repulsion.

# Density has a sharp edge at  $r=R$  (rounded off by the kinetic energy term in the GP eq.)

eda and Huang (1998), and

forces

th repulsive interaction ( $a$  is particularly interesting, satisfied by the parameters  $N$ , current experiments. More corrections of mean-field theory in form (Edwards and Burk, 1996).

ate, the effect of increasing is clearly seen in Fig. 9: the atoms central density becomes rather low. As a consequence, the Gross-Pitaevskii Eq. (39), gives a significant contribution becomes less and less important interaction energy. If one neglects the pressure in Eq. (39), one obtains the form

$$n_{\text{TF}}(\mathbf{r}) = \left[ \frac{2m(\mu - V_{\text{ext}}(\mathbf{r}))}{\hbar^2} \right]^{3/2} \quad (50)$$

$n_{\text{TF}}(\mathbf{r})$ , and  $n=0$  outside. This Thomas-Fermi (TF) approximation

on  $n(\mathbf{r})$  provides the radial profile and number of particles

$$(51)$$

potential depends on the trap potential  $V_{\text{ext}}$  given in Eq. (1). For a harmonic trap, the average  $\omega_{\text{ho}}$  [see Eq. (1)], the energy per particle

This energy is the sum of kinetic and potential energies, since the kinetic energy distribution for large  $N$ . Finally, the energy per particle

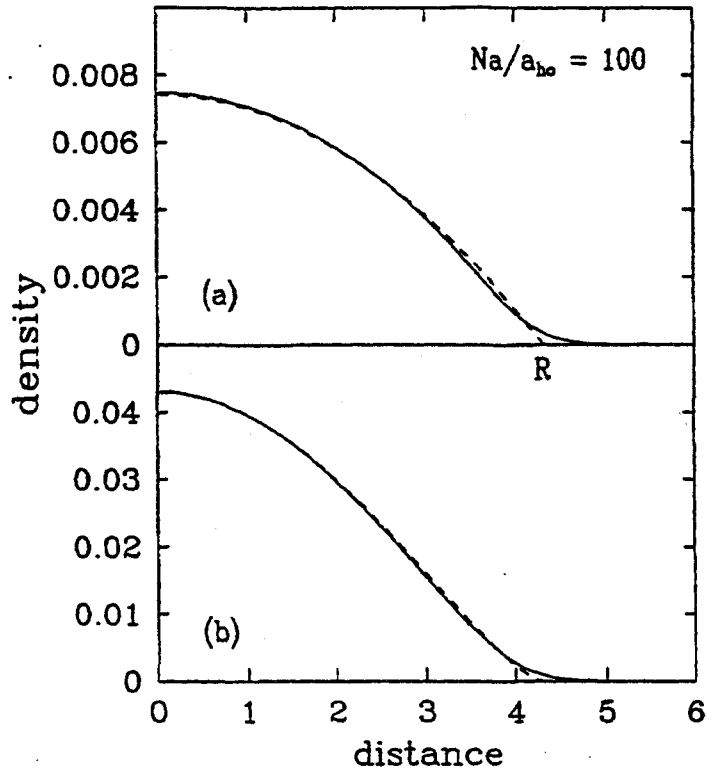


FIG. 13. Density profile for atoms interacting with repulsive forces in a spherical trap, with  $Na/a_{\text{ho}}=100$ . Solid line: solution of the stationary GP Eq. (39). Dashed line: Thomas-Fermi approximation (50). In the upper part, the atom density is plotted in arbitrary units, while the distance from the center of the trap is in units of  $a_{\text{ho}}$ . The classical turning point is at  $R \approx 4.31a_{\text{ho}}$ . In the lower part, the column density for the same system is reported.

trap, this implies  $\mu = m\omega_{\text{ho}}^2 R^2/2$  and, using result (51) for  $\mu$ , one finds the following expression for the radius of the condensate

$$R = a_{\text{ho}} \left( \frac{15Na}{a_{\text{ho}}} \right)^{1/5} \quad (52)$$

which grows with  $N$ . For an axially symmetric trap, the widths in the radial and axial directions are fixed by the conditions  $\mu = m\omega_{\perp}^2 R_{\perp}^2/2 = m\omega_z^2 Z^2/2$ . It is worth mentioning that, in the case of the cigar-shaped trap used at MIT, with a condensate of about  $10^7$  sodium atoms, the axial width becomes macroscopically large ( $Z \sim 0.3$  mm), allowing for direct *in situ* measurements.

The value of the density (50) in the center of the trap is  $n(0) = \left[ \frac{2m(\mu - V_{\text{ext}}(0))}{\hbar^2} \right]^{3/2}$ .

## Attractive forces ( $Q < 0$ )

Central density increases to lower the interaction energy vs. zero point energy to stabilize the gas.

If  $n_0(0)$  too large  $\rightarrow$  KE cannot counteract any longer the collapse at  $N_0 \geq N_{critical} \sim Q_{eff}/|Q|$

$N_{crit}$  from  $\left(\frac{\partial E}{\partial N}\right)_{N_{crit}} = 0$  local minimum in  $N$

above  $N_{crit}$ , the minimum does no longer exist  $\rightarrow$  BP has no solution

#  $N_{crit} \sim \frac{1}{|Q_{eff}|} = .575 \rightarrow {}^7\text{Li}$   $N_{crit} \approx 1400$  consistent with expt.s

#

## MICROSCOPIC THEORIES as in the clusters

CBF + HNC  $\rightarrow \Phi = \prod_{i < j} f(r_{ij}) \prod_e \phi_e(r)$   
 $\uparrow$  g.s. of the non-interacted trap.

CBF + VMC

DMC etc.

# Two length scales (different  $Q_{eff}$  and  $Q$ )  $\rightarrow$  technical difficulties

Use HS potential

Compute the total density  $n(\vec{r})$

Compute the OSDM  $\rightarrow n_0(\vec{r})$  and  $N_0$

Not bound to HS  $\rightarrow$  details of the interaction



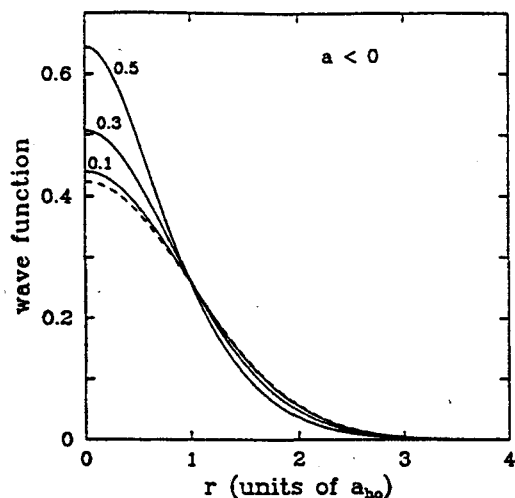


FIG. 8. Condensate wave function, at  $T=0$ , obtained by solving numerically the stationary GP Eq. (39) in a spherical trap and with attractive interaction among the atoms ( $a < 0$ ). The three solid lines correspond to  $N|a|/a_{ho} = 0.1, 0.3, 0.5$ . The dashed line is the prediction for the ideal gas. Here the radius  $r$  is in units of the oscillator length  $a_{ho}$  and we plot  $(a_{ho}^3/N)^{1/2} \phi(r)$ , so that the curves are normalized to 1 [see also Eq. (40)].

interaction and the radius of the atomic cloud consequently increases (decreases). This effect of the interaction has important consequences, not only for the structure of the ground state, but also for the dynamics and thermodynamics of the system, as we will see later on.

The ground state can be easily obtained within the formalism of mean-field theory. For this, one can write the condensate wave function as  $\Phi(\mathbf{r}, t) = \phi(\mathbf{r}) \exp(-i\mu t/\hbar)$ , where  $\mu$  is the chemical potential and  $\phi$  is real and normalized to the total number of particles,  $\int d\mathbf{r} \phi^2 = N_0 = N$ . Then the Gross-Pitaevskii Eq. (35) becomes

$$\left( -\frac{\hbar^2 \nabla^2}{2m} + V_{ext}(\mathbf{r}) + g \phi^2(\mathbf{r}) \right) \phi(\mathbf{r}) = \mu \phi(\mathbf{r}). \quad (39)$$

This has the form of a “nonlinear Schrödinger equation,” the nonlinearity coming from the mean-field term, proportional to the particle density  $n(\mathbf{r}) = \phi^2(\mathbf{r})$ . In the absence of interactions ( $g=0$ ), this equation reduces to the usual Schrödinger equation for the single-particle Hamiltonian  $-\hbar^2/(2m)\nabla^2 + V_{ext}(\mathbf{r})$  and, for harmonic confinement, the ground-state solution coincides, apart from a normalization factor, with the Gaussian function (3):  $\phi(\mathbf{r}) = \sqrt{N} \varphi_0(\mathbf{r})$ . We note, in passing, that a similar nonlinear equation for the order parameter has been also considered in connection with the theory of superfluid helium near the  $\lambda$  point (Ginzburg and Pitaevskii, 1958); in that case, however, the ingredients of the equation have a different physical meaning.

The numerical solution of the GP Eq. (39) is relatively easy to obtain (Edwards and Burnett, 1995; Ruprecht *et al.*, 1995; Dalfovo and Stringari, 1996; Edwards, Dodd *et al.*, 1996b; Holland and Cooper, 1996). Typical wave functions  $\phi$ , calculated from Eq. (39) with different val-

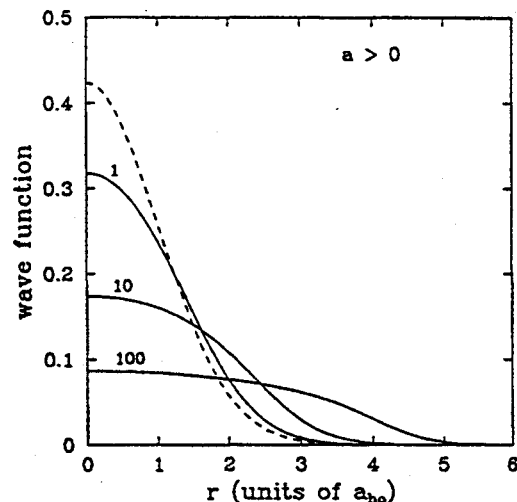


FIG. 9. Same as in Fig. 8, but for repulsive interaction ( $a > 0$ ) and  $Na/a_{ho} = 1, 10, 100$ .

ues of the parameter  $N|a|/a_{ho}$ , are shown in Figs. 8 and 9 for attractive and repulsive interaction, respectively. The effects of the interaction are revealed by the deviations from the Gaussian profile (3) predicted by the non-interacting model. Excellent agreement has been found by comparing the solution of the GP equation with the experimental density profiles obtained at low temperature (Hau *et al.*, 1998), as shown in Fig. 3. The condensate wave function obtained with the stationary GP equation has been also compared with the results of an *ab initio* Monte Carlo simulation starting from Hamiltonian (26), finding very good agreement (Krauth, 1996).

The role of the parameter  $N|a|/a_{ho}$ , already discussed in the previous section, can be easily pointed out, in the Gross-Pitaevskii equation, by using rescaled dimensionless variables. Let us consider a spherical trap with frequency  $\omega_{ho}$  and use  $a_{ho}$ ,  $a_{ho}^{-3}$ , and  $\hbar \omega_{ho}$  as units of length, density, and energy, respectively. By putting a tilde over the rescaled quantities, Eq. (39) becomes

$$[-\tilde{\nabla}^2 + \tilde{r}^2 + 8\pi(Na/a_{ho})\tilde{\phi}^2(\tilde{\mathbf{r}})]\tilde{\phi}(\tilde{\mathbf{r}}) = 2\tilde{\mu}\tilde{\phi}(\tilde{\mathbf{r}}). \quad (40)$$

In these new units the order parameter satisfies the normalization condition  $\int d\tilde{\mathbf{r}} |\tilde{\phi}|^2 = 1$ . It is now evident that the importance of the atom-atom interaction is completely fixed by the parameter  $Na/a_{ho}$ .

It is worth noticing that the solution of the stationary GP Eq. (39) minimizes the energy functional (37) for a fixed number of particles. Since the ground state has no currents, the energy is a functional of the density only, which can be written in the form

$$E[n] = \int d\mathbf{r} \left[ \frac{\hbar^2}{2m} |\nabla \sqrt{n}|^2 + n V_{ext}(\mathbf{r}) + \frac{gn^2}{2} \right] \\ = E_{kin} + E_{ho} + E_{int}. \quad (41)$$

The first term corresponds to the quantum kinetic energy coming from the uncertainty principle; it is usually

Two body cluster energy for N bosons in an harmonic trap

$$H = -\frac{\hbar^2}{2m} \sum_i \nabla_i^2 + \sum_i V_{ext}(r_i) + \sum_{i < j} \delta(r_{ij})$$

$$\Psi = (\prod_i) \phi$$

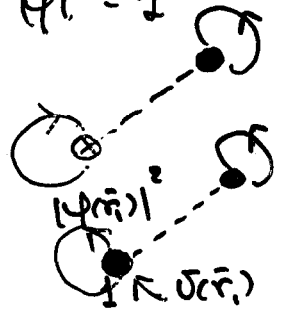
$$\phi = \prod_i \phi(r_i)$$

lowest lying state  
 $\rho(r) = N |\phi|^2$        $\int d^3r |\phi|^2 = 1$

$$\frac{E^v}{N} = T_0 + V_e + V_{JF}$$

$$T_0 = \frac{\hbar^2}{2m} \int d^3r (\nabla \phi)^2$$

$$V_e = \int d^3r |\phi|^2 V_{ext}(r)$$



$$V_{JF} = \frac{N}{2} \int d^3r_1 \int d^3r_2 \phi^2(r_1) \phi^2(r_2) \left[ \underbrace{f(r_{12})}_{V_{JF}(r_{12})} V_{ext} + \frac{\hbar^2}{m} (\nabla f(r_{12}))^2 \right]$$

$|\phi(r)|^2$   
 $(\frac{\hbar^2}{2m} \nabla f)^2$

↓ minimize respect to  $\phi$

$$\left( \frac{\delta E^v}{\delta \phi} \right) = 0$$

$$-\frac{\hbar^2}{2m} \nabla^2 \phi + \left\{ V_{ext} + \int d^3r_1 \phi^2(r_1) V_{JF}(r-\bar{r}_1) \right\} = \mu \phi(r)$$

Correlated Hartree eq. (CHE)

# A Local Density Approximation (LDA)

Start with

$$\frac{E}{N}[\rho] = \frac{1}{N} \frac{\hbar^2}{2m} \int d^3r_1 \sqrt{\bar{\rho}_1} \rho_1^{3/2}(\bar{r}_1) + \frac{1}{N} \int d^3r_1 \rho_1(\bar{r}_1) V_{\text{ext}}(\bar{r}_1) + \frac{E_{\text{con}}[\rho_1]}{N}$$

$$\frac{E_{\text{con}}}{N} = \frac{1}{N} \frac{1}{2} \int d^3r_1 \int d^3r_2 \rho_2(\bar{r}_1, \bar{r}_2) [V(\bar{r}_{12}) - \frac{\hbar^2}{2m} \nabla_1^2 \ln f(\bar{r}_{12})] - \frac{1}{N} \frac{\hbar^2}{2m} \int d^3r_1 \int d^3r_2 \rho_2(\bar{r}_1, \bar{r}_2) \bar{\nabla}_1 \ln f(\bar{r}_{12}) \cdot \bar{\nabla}_1 \rho_1^{3/2}(\bar{r}_1)$$

↓ in LDA

$$\frac{E_{\text{con}}}{N} \approx \frac{E^{\text{LD}}}{N} = \frac{1}{N} \int d^3r_1 \rho_1(\bar{r}_1) E_{\text{con}}^{\text{hom}}[\rho_1(\bar{r}_1)]$$

Energy per particle of the hom. Bose gas at  $\rho_1$ .

Then minimize with respect to  $\bar{\rho}_1$ .

$$\frac{1}{N} E_{\text{con}}^{\text{hom}}(\rho_1) = \frac{E^{\text{HS}}}{N} = \frac{2\pi}{m} \rho_1 a^3 \rightarrow \text{GP equation}$$

$$\frac{E^{\text{HS}}}{N} = \frac{2\pi \hbar^2}{m} \rho_1 a^3 \left[ 1 + \frac{128}{15} \left( \frac{\rho_1 a^3}{\sqrt{\pi}} \right)^{3/2} \right] \rightarrow \text{MGP equation}$$

$$\left[ -\frac{1}{2} \nabla^2 + \frac{1}{2} \bar{r}^2 + 4\pi \bar{\rho} N \bar{\rho}_1(\bar{r}) + 5\pi^{1/2} \bar{\rho}^{3/2} N^{3/2} \frac{128}{15} \bar{\rho}_1^{3/2}(\bar{r}) \right] \sqrt{\bar{\rho}_1(\bar{r})} =$$

$$= \mu \sqrt{\bar{\rho}_1(\bar{r})}$$

in reduced unities

$$\rho_1(\bar{r}) = \frac{N}{\Omega^3} \bar{\rho}_1(\bar{r})$$

$$\bar{a} = a/a_{ho}$$

$$\bar{r} = \bar{r}/a_{ho}$$

$$\bar{\mu} = \mu/\hbar\omega$$

HGP eq.  $\rightarrow$  corrections in  $x^{1/2}$  from LDA to  $E_{\text{con}}$

A consistent version (Broaten and Niets)

contains corrections to the kinetic energy term  
(very small)

$$\text{if } \frac{E_{\text{con}}^{\text{hom}}}{N}(\rho_i) = \frac{E_{\text{con}}^{\text{HNC}}}{N}(\rho_i) \quad \text{from CBF/HNC}$$

then  $\rightarrow$  Correlate Hartree eq. (CH)

$$\left[ -\frac{1}{2} \nabla^2 + \frac{1}{2} \bar{r}^2 + E^{\text{HNC}}(x) + x \frac{\partial E^{\text{HNC}}(x)}{\partial x} \right] \psi_{\rho_i}(\bar{r}) = \mu \psi_{\rho_i}(\bar{r})$$

where  $x(\bar{r})$  is the local gas parameter

$$x(\bar{r}) = \rho_i(\bar{r}) a^3$$

HGP and CH eqs connect GP at large  $x$ -values

↓

Regions where corrections to the GP approach  
are visible within experimental reach

TABLE I. Chemical potentials  $\mu_1$ , ground-state energies per particle  $E_1/N$ , and root mean-square radii  $R_{rms}$ , of  $N$   $^{87}\text{Rb}$  atoms in an isotropic trap ( $\omega/2\pi=77.78$  Hz) in TF approximation or solving the GP [Eq. (2)], the MGP [Eq. (5)], and the correlated Hartree HNC [Eq. (17)] equations. The  $N=1.5\times 10^7$  row refers to the Na case ( $\omega/2\pi=230$  Hz). Energies are in units of  $\hbar\omega$  and lengths are in units of  $a_{HO}$ .

$N$	$\mu_1$				$E_1/N$				$R_{rms}$		
	TF	GP	MGP	HNC	TF	GP	MGP	HNC	GP	MGP	HNC
$10^3$	2.66	3.04	3.06	3.04	1.90	2.43	2.43	2.43	1.65	1.66	1.66
$10^4$	6.67	6.87	6.92	6.89	6.87	5.04	5.08	5.04	2.44	2.45	2.44
$10^5$	16.75	16.85	17.07	16.94	11.96	12.10	12.25	12.20	3.80	3.84	3.83
$10^6$	42.07	42.12	42.97	42.53	30.05	30.12	30.66	30.48	6.01	6.10	6.06
$10^7$	105.68	105.70	108.75	107.20	75.49	75.52	77.48	76.85	9.52	9.74	9.64
$1.5\times 10^7$	91.07	91.10	92.41	91.67	65.05	65.09	65.92	65.66	8.84	8.92	8.90
$10^8$	265.46	265.47	275.89	273.58	189.61	189.63	196.45	194.74	15.08	15.44	15.38

where we have again introduced the scaled unities and the local gas parameter,  $x_{loc}(\vec{r}) = \rho_1(\vec{r})a^3 = N\bar{a}^3|\psi_1(\vec{r})|^2$ .

The calculations have been performed for the  $^{87}\text{Rb}$  scattering length. The scaled energies per particle and the root mean-square radii are reported in Table I for particle numbers from  $10^3$  to  $10^8$ . The table also shows the results obtained by neglecting the kinetic-energy term in the Gross-Pitaevskii equation. This approach, loosely called the Thomas-Fermi (TF) approximation, has been discussed in the literature and allows for deriving simple analytical expressions [10]. The differences between this Thomas-Fermi approach and a rigorous one have been recently discussed [21,22] for spatially inhomogeneous Bose condensates. Local-density approximation has been used [1,5] to estimate corrections to the Gross-Pitaevskii for the ground and excited states within the Thomas-Fermi approximation and retaining only the first correction in Eq. (1). The second correction is negative and partially cancels the first one. For instance, the cancellations go from  $\sim 15\%$  for  $N=10^4$  to  $\sim 40\%$  at  $N=10^6$  if we just take the central densities, whereas the final energy is reduced by  $\sim 15\%$  at  $N=10^6$  and it is practically unaffected by the second correction at lower  $N$  values.

As expected, the Thomas-Fermi results are close to the Gross-Pitaevskii ones when  $N$  becomes large. The differ-

ences between GP and MGP increase with the number of particles and are of the order of 4% for the chemical potential and 2.5% for the energy at  $N=10^7$ . The higher-order terms in the low-density expansion always have a repulsive effect. The same behavior is shown by the HNC results, which, however, are less repulsive than MGP at the large  $N$  values.

We notice that if one uses the Gross-Pitaevskii solution to perturbatively estimate the MGP energy, then the correction is negative (at  $N=10^7$ ,  $\Delta E_1 = -4.54$ ). The nonlinear character of Eq. (5) is responsible for this discrepancy.

The density profile (normalized to unity) for  $N=10^7$  particles is given in Fig. 2. For this large number of particles the TF and GP densities are close, whereas the more repulsive MGP and HNC solutions lower the central density, expanding the density distribution and providing a larger radius, as shown in Table I.

We have also considered a system of  $N=1.5\times 10^7$  Na atoms ( $a=27.5$  Å) in a spherical trap having a frequency of 230 Hz. These conditions roughly correspond to those of the experiment described in Ref. [4]. The results are shown in the last row of the table and in Fig. 2. The effects of the correlations are similar to those found in the large  $N$  Rb cases. The energy increases by  $\sim 1\%$  and the rms radius by  $\sim 0.7\%$  respect to GP. The HNC central density is slightly reduced.

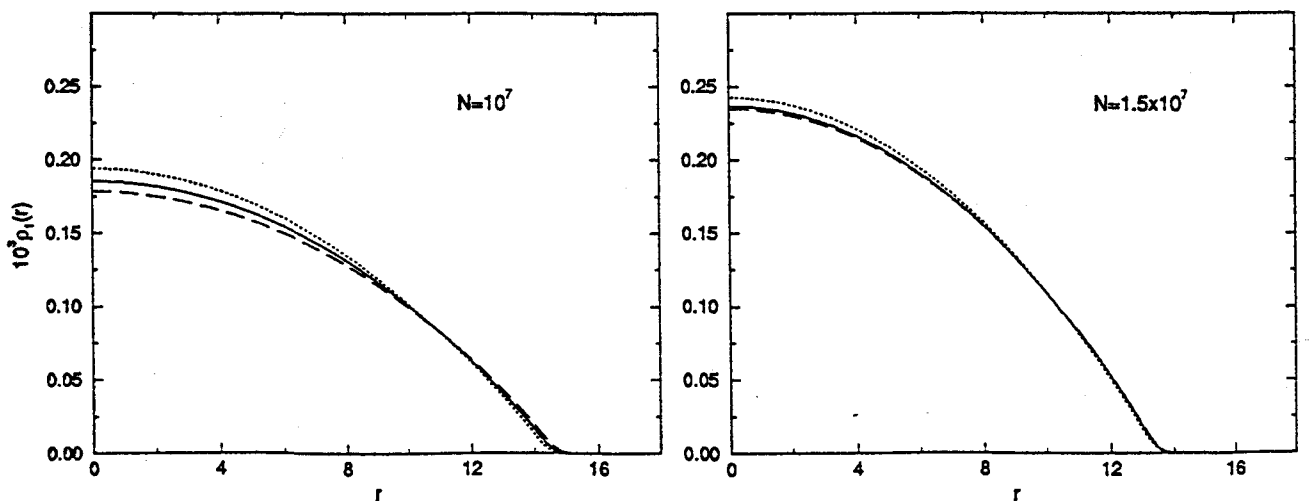


FIG. 2. Density profiles for  $N=10^7$  Rb atoms and for  $N=1.5\times 10^7$  Na atoms in different approaches (dotted line, Gross-Pitaevskii; dashed line, modified Gross-Pitaevskii; solid line, hypernetted chain). Densities are normalized to unity and distances are in units of  $a_{HO}$ .

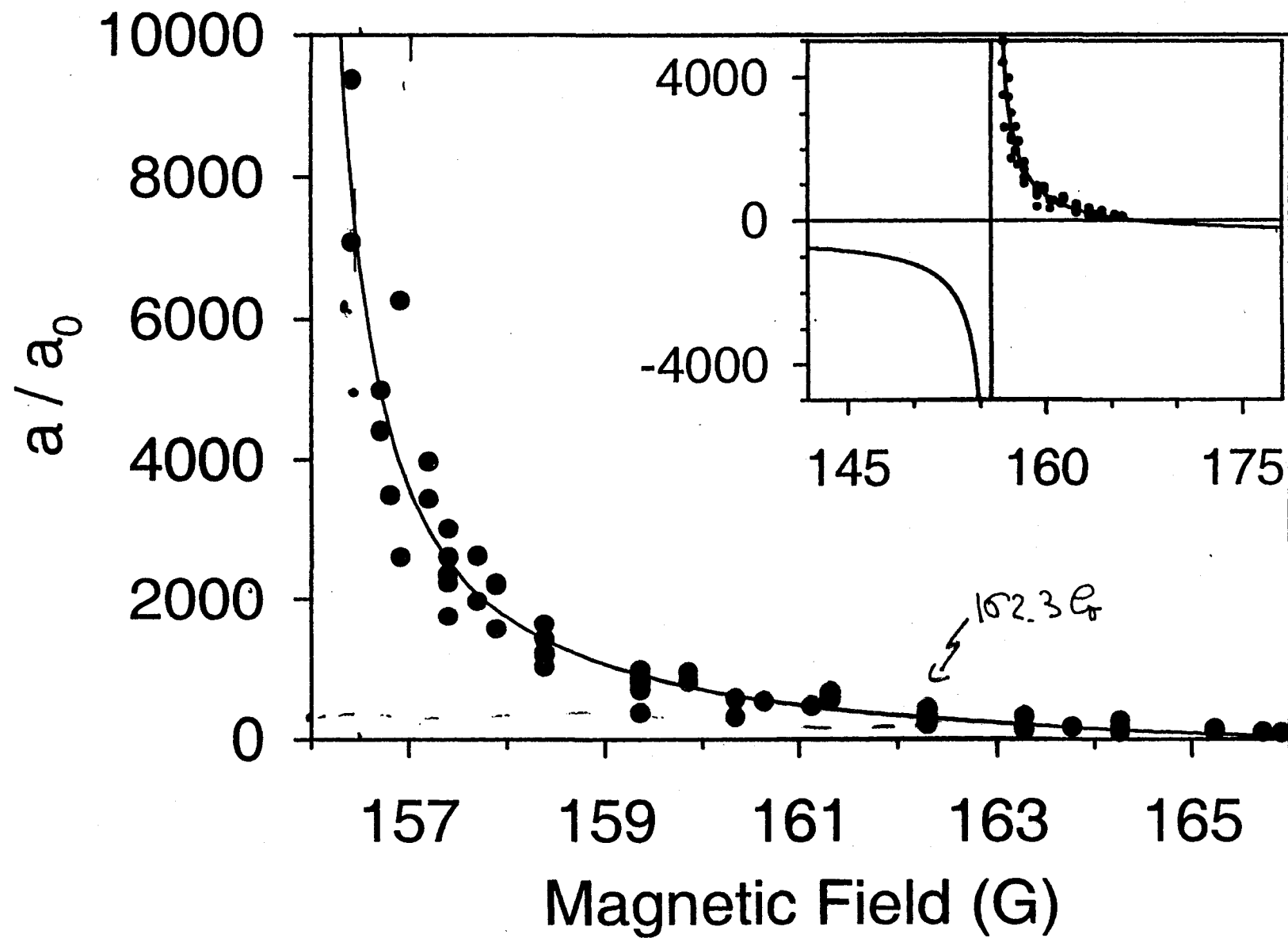
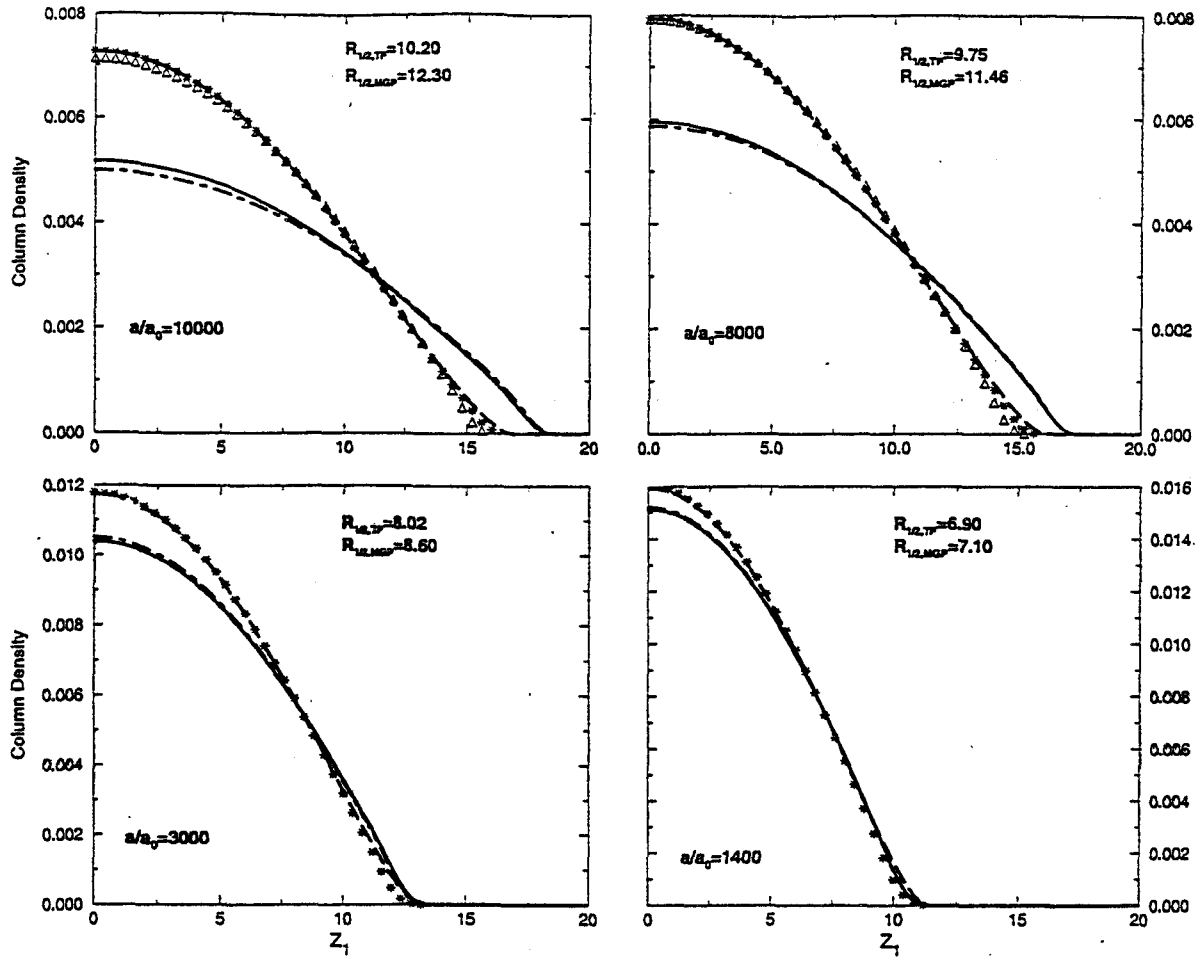


TABLE II. Ground state properties of  $N = 10^4$   $^{85}\text{Rb}$  atoms in the cylindrical trap described in the paper. Energies in HO units.

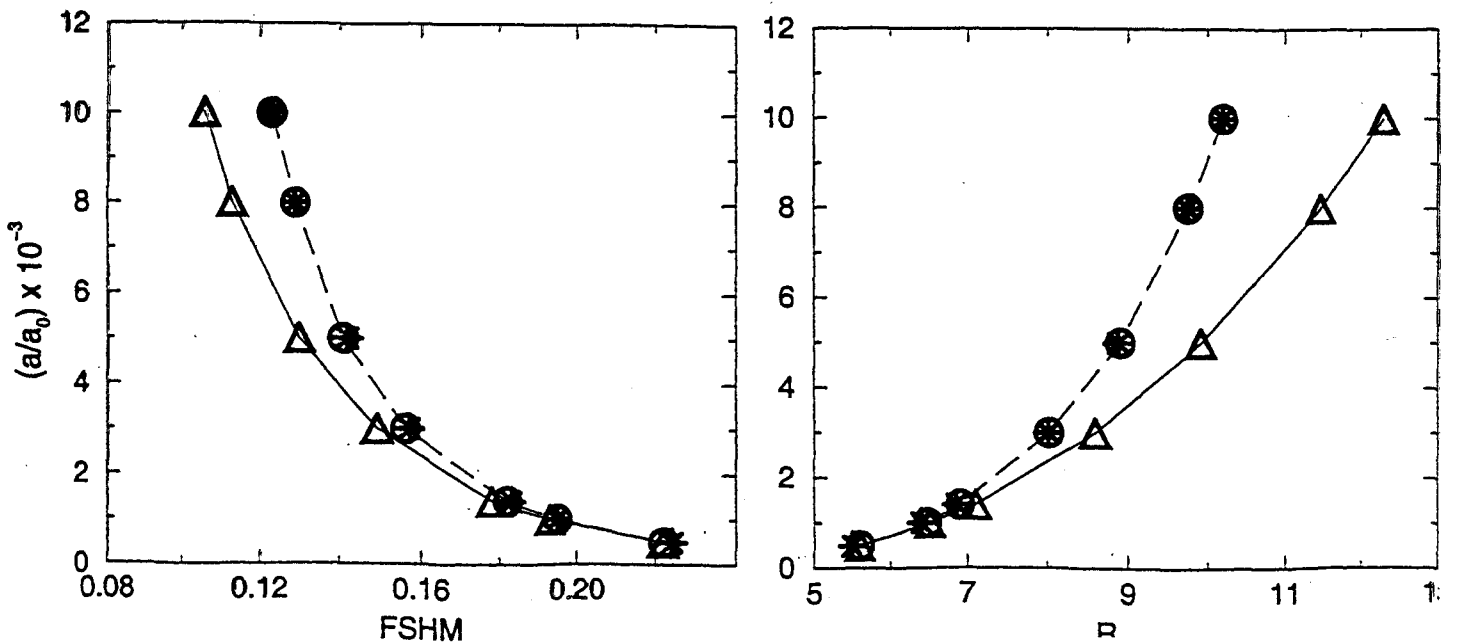
$a/a_0$	1400	3000	8000	10000
$\mu_1^{TF}$	9.70	13.15	19.47	21.29
$\mu_1^{GP}$	9.82	13.25	19.55	21.36
$\mu_1^{MGP}$	10.22	14.51	24.38	27.79
$\mu_1^{CBF}$	10.19	14.38	24.37	28.09
$E_1^{TF}/N$	6.93	9.39	13.91	15.21
$E_1^{GP}/N$	7.08	9.52	14.00	15.29
$E_1^{MGP}/N$	7.33	10.31	17.09	19.43
$E_1^{CBF}/N$	7.31	10.23	16.98	19.42
$x_{pk}^{TF}$	$6.23 \times 10^{-4}$	$3.88 \times 10^{-3}$	$4.09 \times 10^{-2}$	$6.98 \times 10^{-2}$
$x_{pk}^{GP}$	$6.28 \times 10^{-4}$	$3.90 \times 10^{-3}$	$4.10 \times 10^{-2}$	$7.00 \times 10^{-2}$
$x_{pk}^{MGP}$	$5.72 \times 10^{-4}$	$3.19 \times 10^{-3}$	$2.60 \times 10^{-2}$	$4.10 \times 10^{-2}$
$x_{pk}^{CBF}$	$5.76 \times 10^{-4}$	$3.24 \times 10^{-3}$	$2.53 \times 10^{-2}$	$3.86 \times 10^{-2}$



FIGURES

FIG. 1. Column densities at four values of the scattering length for the cylindrical trap. Dashed lines= TF, stars= GP, solid lines= MGP, dot-dashed lines= CBF. The triangles in the first (second) upper panel give the MGP column density at  $a/a_0=5920$  (4940).

FIG. 2. Scattering length as a function of the full strength at half maximum (left) and of the half maximum radius (right) in the cylindrical trap. Circles, stars and triangles correspond to the TF, GP and MGP results, respectively. Lines are a guide to the eyes.





## Other relevant topics

- 1) Excitations ( $t$ -dependent GP)
  - 2) Sum rules and collective excitations (AP)
  - 3) Thermodynamics
  - 4) BEC and superfluidity
  - 5) Vortices
  - 6) Interference etc.
- 7) Mixture of boson species ( $^{85}\text{Rb}$ - $^{87}\text{Rb}$ ,  $^7\text{Li}$ - $^6\text{Li}$ )  
BB BF

Dalfovo et al. RMP 71 (1999) 463

#

Study of BEC in homogeneous and inhomogeneous systems is a challenge to many-body physics.

Reliability of QMB techniques can be TESTED against expt.?